Biomedicine & Pharmacotherapy 156 (2022) 113982

Contents lists available at ScienceDirect

Biomedicine & Pharmacotherapy

journal homepage: www.elsevier.com/locate/biopha

Eleutheroside B ameliorated high altitude pulmonary edema by attenuating ferroptosis and necroptosis through Nrf2-antioxidant response signaling

Yilan Wang [a,1], Zherui Shen [a,1], Caixia Pei [a], Sijing Zhao [a], Nan Jia [a], Demei Huang [a], Xiaomin Wang [a], Yongcan Wu [a], Shihua Shi [a], Yacong He [b,*,2], Zhenxing Wang [a,*,2]

[a] Hospital of Chengdu University of Traditional Chinese Medicine, No. 39 Shi-er-qiao Road, Chengdu, Sichuan 610075, China
[b] School of Pharmacy, Chengdu University of Traditional Chinese Medicine, No.1166 Liutai Avenue, Chengdu, Sichuan 611137, China

ARTICLE INFO

Keywords:
Eleutheroside B
High-altitude pulmonary edema
Nrf2
Ferroptosis
Necroptosis
Oxidative stress

ABSTRACT

High altitude pulmonary edema (HAPE) is a potentially fatal condition induced by exposure to high-altitude environment. Eleutheroside B is a naturally active polyphenolic substance that has previously demonstrated anti-inflammatory, antioxidant and antidepressant properties. However, the effects of eleutheroside B on HPAE are unknown. Here, eleutheroside B (50 mg/kg and 100 mg/kg) was applied to HAPE rats. Eleutheroside B alleviated lung edema and decreased levels of tumor necrosis factor-α, interleukin-1β, vascular endothelial growth factor, and total proteins in the bronchoalveolar lavage fluid. Eleutheroside B reversed the acid-base disturbances by HAPE. In addition, eleutheroside B reversed the oxidative stress. Eleutheroside B pretreatment facilitated the translocation of nuclear factor E2-related factor 2 (Nrf2) into the nucleus, contributing to the inhibition of ferroptosis and necroptosis. ML385 confirmed the role of Nrf2 in ferroptosis and necroptosis. Collectively, the beneficial effects of eleutheroside B against HAPE were associated with the inhibition of ferroptosis and necroptosis through Nrf2-antioxidant response signaling.

1. Introduction

High-altitude pulmonary edema (HAPE) is a non-cardiogenic form of pulmonary edema that develops in unacclimatized individuals at altitudes over 2500 m [1]. High-altitude hypobaric hypoxia induces pulmonary vasoconstriction and capillary leak, resulting in increased pulmonary pressure and edema fluid accumulation in the alveolar spaces [2]. The incidence of HAPE in healthy individuals is 0.01 % at altitudes greater than 2500 m [3]. In a Chinese study, 0.49 % of individuals who went up to 5000 m were diagnosed with HAPE [4]. Dry cough and reduced exercise capacity represent the earliest symptoms of HAPE. As the disease progresses, patients may experience shortness of breath, expectoration, cyanosis, palpitations and syncope [5]. Currently, gradual ascent is the primary recommended method for preventing HAPE. However, pharmacological interventions can also be used, including acetazolamide, dexamethasone, calcium channel blockers, and phosphodiesterase inhibitors. Patients with HAPE who fail to receive a correct diagnosis and timely treatment have a mortality rate up to 40 % [6]. Until now, the pathogenesis of HAPE has not been clarified, and it lacks an effective predictive index and treatment scheme.

Abbreviations: BALF, bronchoalveolar lavage fluid; CAT, catalase; COX2, cyclooxygenase 2; FTH1, ferritin heavy chain 1; GPX4, glutathione peroxidase 4; HAPE, high altitude pulmonary edema; Hb, hemoglobin; HCO3, bicarbonate; Hct, hematocrit; HO-1, heme oxygenase-1; H&E, hematoxylin and eosin; IL-1β, interleukin-1β; Nrf2, nuclear factor E2-related factor 2; Keap1, kelch-like ECH-associated protein 1; MDA, malondialdehyde; MLKL, mixed lineage kinase domain-like; NF-κB, nuclear factor-κB; NOX1, nicotinamide adenine dinucleotide phosphate oxidase 1; PaCO2, partial pressure of carbon dioxide; PaO2, partial pressure of oxygen; PBS, phosphate buffered saline; pH, potential of hydrogen; RIPK1, receptor-interacting protein kinase 1; RIPK3, receptor-interacting protein kinase 3; ROS, reactive oxygen species; SaO2, arterial oxygen saturation; SLC7A11, solute carrier family 7 member 1; TEM, transmission electron microscopy; TFRC, transferrin receptor; TNF-α, tumor necrosis factor-α; VEGF, vascular endothelial growth factor; W/D, wet-to-dry; 4-HNE, 4-hydroxynonenal.

* Corresponding authors.
E-mail addresses: wangyilan@stu.cdutcm.edu.cn (Y. Wang), shenzherui1216@163.com (Z. Shen), 2297316104@qq.com (C. Pei), zhaosijing@stu.cdutcm.edu.cn (S. Zhao), jn18215620918@163.com (N. Jia), huangdemei@stu.cdutcm.edu.cn (D. Huang), waugxuaomin@163.com (X. Wang), appleofcan@163.com (Y. Wu), Shi_shihua@163.com (S. Shi), heyacong@126.com (Y. He), wangzhenxing@cdutcm.edu.cn (Z. Wang).
[1] Yilan Wang and Zherui Shen contributed equally to this study.
[2] Zhenxing Wang and Yacong He are the co-corresponding authors.

https://doi.org/10.1016/j.biopha.2022.113982
Received 14 September 2022; Received in revised form 31 October 2022; Accepted 4 November 2022
Available online 7 November 2022

Reactive oxygen species (ROS) are a group of highly unstable oxygen-derived molecules, including free radicals and oxygen peroxides. Accumulation of ROS is involved in the progression of HAPE [7]. The nuclear factor E2-related factor 2 (Nrf2) is a transcriptional factor that regulates the expression of several antioxidant proteins. Under physiological conditions, Nrf2 and Kelch-like ECH-associated protein 1 (Keap1) are bound to each other in the cytosol. When oxidative stress occurs, Nrf2 translocates into the nucleus and induces the expression of ROS-detoxifying enzymes, preventing ROS accumulation [8]. The Nrf2 activation effectively attenuated ROS production and alleviated brain vascular leak in a rat model of HAPE [9]. Previous literature reported that Nrf2 up-regulation could be recommended as an effective alternative treatment in high altitude sickness [9]. As an antioxidant transcription factor, the intracellular molecular mechanisms of Nrf2 transcription and translation have not been fully elucidated in HAPE.

Ferroptosis is a form of non-apoptotic cell death characterized by the accumulation of intracellular iron and lipid peroxidation. Besides, the mitochondrial tricarboxylic acid (TCA) cycle plays a significant role in ROS accumulation, which could induce ferroptosis. The main driver of such mitochondrial-derived ROS is an ischemic accumulation of the TCA cycle metabolite succinate [10]. In C57BL/6 mice, acute hypobaric hypoxia could induce neuronal ferroptosis [11]. An increased expression of Nrf2 inhibited ferroptosis via reducing ROS accumulation [12]. Necroptosis is a non-apoptotic form of programmed cell death that plays an important role in many inflammatory conditions, including hypoxia [13]. Necroptosis is regulated by receptor-interacting protein kinase 1 (RIPK1) and 3 (RIPK3). In liver injury, the downregulation of Nrf2 aggravated necroptosis [14]. Concerning ferroptosis and necroptosis in HAPE, there has been no study reported in the literature, and such research is worthy of more attention. The modulation of ferroptosis and necroptosis might be therapeutic against HAPE.

Eleutheroside B is a naturally active polyphenolic substance derived from *Eleutherococcus senticosu,* a plant commonly used to prevent altitude sickness. Eleutheroside B has previously demonstrated antidepressant, anti-tumor, anti-inflammatory, and antioxidant properties [15–18]. Eleutheroside B attenuated lung injury by upregulating Nrf2 and inhibiting oxidative stress [19]. Furthermore, eleutheroside B suppressed the expression of RIPK1 and RIPK3, which are critical signaling molecules in necroptosis [20]. The potential effects of eleutheroside B against HAPE are currently unknown. Therefore, the pathological mechanism of HAPE needs to be further explored, as well as the therapeutic effects of eleutheroside B. The present study was designed to address the above concerns via experiments in vivo.

2. Materials and methods

2.1. Reagents

Eleutheroside B (HPLC $\geq$ 98 % purity by high-performance liquid chromatography analysis) was obtained from Chengdu Manster Biotechnology Co., Ltd. (Chengdu, China). ML385 and acetazolamide were provided by Selleck Chemicals (Houston, USA). ROS content in rat lung tissues was measured using the ROS determination kit (Beyotime, Shanghai, China). Enzyme-linked immunosorbent assay (ELISA) kits detecting tumor necrosis factor-α (TNF-α), interleukin-1β (IL-1β), 4-hydroxynonenal (4-HNE), tissue iron, malondialdehyde (MDA), catalase (CAT) and vascular endothelial growth factor (VEGF) levels were obtained from Nanjing Jiancheng Bioengineering Company (Nanjing, China). Arterial blood gas test strips were provided by EPOC, Siemens Healthcare (Ottawa, Canada). Horseradish peroxidase-conjugated goat anti-rabbit IgG secondary antibodies were provided by Biodragon Immunotechnologies Co., Ltd. (Beijing, China). Antibodies binding to Nrf2, glutathione peroxidase 4 (GPX4), nicotinamide adenine dinucleotide phosphate oxidase 1 (NOX1), heme oxygenase-1 (HO-1), Lamin B, and β-actin were purchased from Abcam Inc. (Cambridge, UK). Antibodies binding to solute carrier family 7 member 1 (SLC7A11), transferrin receptor (TFRC), RIPK1, RIPK3, mixed lineage kinase domain-like (MLKL), and phospho-MLKL were provided by ABclonal Biotechnology Co., Ltd. (Wuhan, China). Antibodies binding to cyclooxygenase 2 (COX2) and ferritin heavy chain 1 (FTH1) were obtained from Cell Signaling Technology (Danvers, US). The nuclear and cytoplasmic protein extraction kit was obtained from Solarbio Biological Technology Co., Ltd. (Beijing, China). The Pierce™ bicinchoninic acid (BCA) protein assay kit was purchased from Thermo Fisher Scientific (Waltham, USA).

2.2. Animals

Sprague-Dawley rats (male, six-week-old, weighing between 160 and 180 g) were purchased from Chengdu Dashuo Experimental Animal Co., Ltd. (Chengdu, China). After a week of adaptive feeding, the experiments were performed at 22 °C under a light/dark cycle of 12 h/12 h and humidity at 55 ± 5 %. Rats were maintained on a standard pellet diet and water ad libitum. The experimental protocol was approved by the Ethics Committee of Chengdu University of Traditional Chinese Medicine (Grant No. 2022–18). Experimental procedures were conducted in compliance with the Guide for the Care and Use of Laboratory Animals, and the ARRIVE guidelines (Animal Research: Reporting of In Vivo Experiments).

2.3. Experimental design

In the phase I of the research, 35 rats were randomly allocated into 5 groups of 7 animals. The group 1 served as a normoxia control group (0 h). The other groups were exposed to hypobaric hypoxia for different time intervals: 12 h, 24 h, 36 h and 48 h.

In the phase II of the research, 42 rats were randomly distributed into six groups (n = 7 per group): normoxia control (NC), eleutheroside B (EB, 100 mg/kg), hypobaric hypoxia model (HHM), eleutheroside B 50 (EB, 50 mg/kg), eleutheroside B 100 (EB, 100 mg/kg), and acetazolamide (AZ, 50 mg/kg). Acetazolamide was used as a positive control drug based on its protective role against hypobaric hypoxia. The dosages of eleutheroside B and acetazolamide were chosen according to previously published literature [21,22]. According to the protocols provided by the manufacturer, eleutheroside B was dissolved in a solvent composed of 30 % polyethylene glycol 300 (PEG300) + 66% double-distilled water (ddH2O) + 2% dimethyl sulfoxide (DMSO) + 2 % Tween 80. Rats received an intraperitoneal injection of corresponding medications once daily for three consecutive days. Rats in the NC and HHM groups were administered with an equal volume of normal saline. After intraperitoneal administrations, rats in the HHM, EB50, EB100, and AZ groups were exposed to hypobaric hypoxia. Rats in the NC and EB groups were remained at normoxia conditions (500 m altitude).

In the phase III of the research, 28 rats were divided into 4 groups (n = 7 per group): hypobaric hypoxia model (HHM), eleutheroside B 100 (EB, 100 mg/kg), hypobaric hypoxia model + ML385 (HHM + ML385) and eleutheroside B 100 + ML385 (EB100 mg/kg + ML385). ML385 is an Nrf2 inhibitor that was dissolved in a solvent mixture composed of 5 % Tween80 + 40 % polyethylene glycol 300 (PEG300) + 50 % ddH_2O + 5 % dimethyl sulfoxide (DMSO). ML385 (30 mg/kg) was intraperitoneally administered 1 h prior to hypobaric hypoxia exposure in the HHM + ML385 and EB100 + ML385 groups. The dosage of ML385 was determined according to a previous in vivo study [23]. The other groups received treatments similar to the phase II. At the termination of the experiment, rats were euthanized by an intraperitoneal injection of sodium pentobarbital.

2.4. HAPE modeling

Rats were placed in a low-pressure hypoxia animal system (ProOx-830, Shanghai Tawang Intelligent Technology). The system was equipped with a pump, a cabin, a pipeline oxygen supply, connecting pipes,

and communication systems mimicking a high-altitude environment [24]. The temperature and humidity were maintained at 25 °C and 55 %, respectively. The altitude was set to 6000 m with a height rising rate of 20 m/s. During ascending, sodium lime was used to prevent the CO2 concentration from rising too high. Our phase I results revealed that hypobaric hypoxia caused the most obvious changes of Nrf2 translocation at 48 h, the duration of hypobaric hypoxia exposure was set to 48 h in the phase II and phase III of the research. Meanwhile, the duration of hypobaric hypoxia exposure was referenced to previously published literature [25]. Food and water were freely accessible during hypobaric hypoxia exposure. The pain of experimental animals was minimized by taking appropriate measures. After modeling, rats were removed from the experimental cabin and immediately anesthetized by an intraperitoneal injection of sodium pentobarbital.

2.5. Lung wet/dry weight ratio

After sacrifice, the upper lobe of the right lung was excised. The wet weight was measured and recorded using electronic scales. Subsequently, the dry weight was obtained after being dried in an oven at 60 °C for 72 h. To assess edema, we determined the wet/dry weight (W/D) ratio of the upper lobe of the right lung.

2.6. Lung histopathology

The middle lobe of the right lung was extracted, washed, and fixed in buffered 4% paraformaldehyde solution (v/v) for 12 h at 4 °C. The lung tissues were then dehydrated with a sequence of ethanol solutions, embedded in paraffin, and cut into slices (4 μm thickness). The obtained sections were stained with hematoxylin and eosin (H&E) and examined under an optical microscope (OLYMPUS BX41, Japan). Histological scoring was conducted by two expert pathologists in a blinded manner [26].

2.7. Arterial blood gas analysis

After anesthesia, the abdominal cavity of rats was opened and blood was collected from the abdominal aorta into standard sampling tubes containing lithium heparin. Then, 0.1 mL of blood was measured with a blood gas analyzer (EPOC, Siemens Healthcare) to obtain arterial oxygen saturation (SaO_2), partial pressure of oxygen (PaO_2), hematocrit (Hct), hemoglobin (Hb), potential of hydrogen (pH), partial pressure of carbon dioxide ($PaCO_2$) and bicarbonate (HCO_3).

2.8. Determination of levels of TNF-α, IL-1β, VEGF, and total proteins in bronchoalveolar lavage fluid (BALF)

The right lung were ligated, while the left lung was lavaged twice by using 0.5 mL of precooled PBS via a tracheal cannula. The washing liquid obtained was collected, mixed, and centrifuged (3000 rpm for 10 min at 4 °C), then the supernatant was frozen at − 80 °C for further analysis. We measured TNF-α, IL-1β, and VEGF levels in BALF using appropriate ELISA kits. The total protein concentration in BALF was determined by using a BCA protein estimation kit. The optical density was measured using an auto-microplate reader (Thermo Fisher Scientific, Inc.).

2.9. Quantification of MDA, CAT, 4-HNE, and iron in lung tissues

Parts of the right lung tissues of rats were removed and cleaned with aseptic saline. The lung tissues were then homogenized with PBS and centrifuged (12,000 rpm for 15 min at 4 °C) to obtain supernatants for subsequent analysis. Several assay kits were used to measure the levels of MDA, CAT, 4-HNE, and iron in lung tissues. The total protein content of tissue extracts was determined using the BCA protein assay kit. The optical density was measured using an auto-microplate reader (Thermo Fisher Scientific, Inc.).

2.10. Determination of intracellular ROS

The lung tissues were minced into 2–4 mm pieces using sterilized scalpels and scissors. Then, the minced tissues were digested in 0.2 % collagenase type 2 and PBS for 2 h at 37 °C. The cell suspensions were filtered through 200-mesh cell sieves to remove the connective tissues. The suspensions were centrifuged (300 rpm for 5 min at 4 °C) and the supernatant was discarded. Following two washes with PBS, cells were resuspended in flow buffer. Cells were counted and the density was adjusted to 1×10^7 cells/mL. The cells were later collected and suspended in diluted DCFH-DA (1:1000 with the serum-free medium) with a concentration of approximately 1×10^6 cells/mL, then incubated for 20 min in a 5% CO_2 incubator at 37 °C. The flow cytometry was utilized to measure intracellular ROS levels after washing the cells three times with serum-free cell culture medium. Quantitative analyses were performed using a Beckman Coulter flow cytometer (Beckman Coulter, USA).

2.11. Transmission electron microscopy

The apex of the left lung was excised, fixed with 3% glutaraldehyde, and post-fixed with 1% osmium tetroxide. Then, the tissue samples were dehydrated through an acetone series and embedded in an epoxy resin (Epon 812). Ultrathin sections were stained with uranyl acetate and lead citrate. The transmission electron microscopy (TEM) images of ultrathin sections were captured with a JEM-1400Flash transmission electron microscopy (Tokyo, Japan).

2.12. Immunofluorescence analysis of lung tissue

Lung tissues were embedded in paraffin and sliced into 4-μm sections. The sections were deparaffinized with xylene and subsequently rehydrated with graded alcohol. The sections were then incubated with 0.3 % hydrogen peroxide for 15 min to quench endogenous peroxidase and later incubated with 10% normal goat serum for 10 min to block nonspecific immunoglobulin binding. Antigen retrieval was conducted by boiling sections in 0.01 M sodium citrate buffer (pH 6.0) for 10 min. After that, sections were incubated overnight with primary antibodies binding to Nrf2, GPX4, and RIPK3. The following day, the sections were incubated with secondary antibodies for 1 h at room temperature. Lastly, the sections were stained with 4,6-diamino-2-phenyl indole (DAPI) for 15 min to label cell nuclei, and images were recorded using a fluorescence microscope (OLYMPUS, BX51, Japan). The quantitative measurement of fluorescent intensity was performed by Image J software.

2.13. Nuclear and cytosolic protein extraction

Part of the left lung was removed and cut into fine fragments. Cell suspensions were obtained from tissue samples by using a homogenizer with cooled PBS on ice. The suspensions were then centrifuged (500 rpm for 3 min at 4 °C) and the supernatant was discarded. The precipitates were collected and a cytosolic protein extraction agent was added. After suspension being incubated in an ice bath and centrifuged, the supernatant was stored as cytosolic protein samples. Further precipitates were collected and a nuclear protein extraction agent was added. After incubation in an ice bath, vortex oscillation, and centrifugation, the supernatant was stored as nuclear protein samples. The cytosolic and nuclear protein samples were harvested and stored at − 70 °C for subsequent analysis.

2.14. Western blotting

Tissues from sacrificed rats were collected, frozen in liquid nitrogen

immediately, and stored at − 80 °C until further analysis. The lung tissues were lysed with the radio-immunoprecipitation assay (RIPA) lysis buffer containing protease inhibitors, a phosphatase inhibitor cocktail, and 1 mM phenylmethylsulfonyl fluoride (PMSF). After centrifugation (12,000 rpm for 10 min at 4 °C) of the homogenates, the supernatant was collected as protein samples. The protein concentration was determined using a BCA protein assay kit. Proteins with different molecular weights were separated with a 8–15 % (w/v) sodium dodecyl sulfate-polyacrylamide gel electrophoresis (SDS-PAGE). Subsequently, proteins were transferred to polyvinylidene difluoride (PVDF) membranes that were blocked with 5 % bovine calf serum (BSA) or 5 % skim milk in tris-buffered saline (TBS) with 0.01% tween 20. After blocking for 1 h, membranes were incubated overnight at 4 °C with primary antibodies binding to Nrf2, NOX1, GPX4, HO-1, SLC7A11, TFRC, RIPK1, RIPK3, phospho-MLKL, MLKL, COX2, FTH1, lamin B, and β-actin. On the second day, PVDF membranes were incubated with appropriate secondary antibodies for 2 h at room temperature. The chemiluminescence substrate was applied to visualize the protein bands. Images were captured using a Bio-Rad image analysis system (Bio-Rad, USA). The β-actin or lamin B was used as the loading control and the relative protein expression was analyzed by Image-Pro Plus software 6.0.

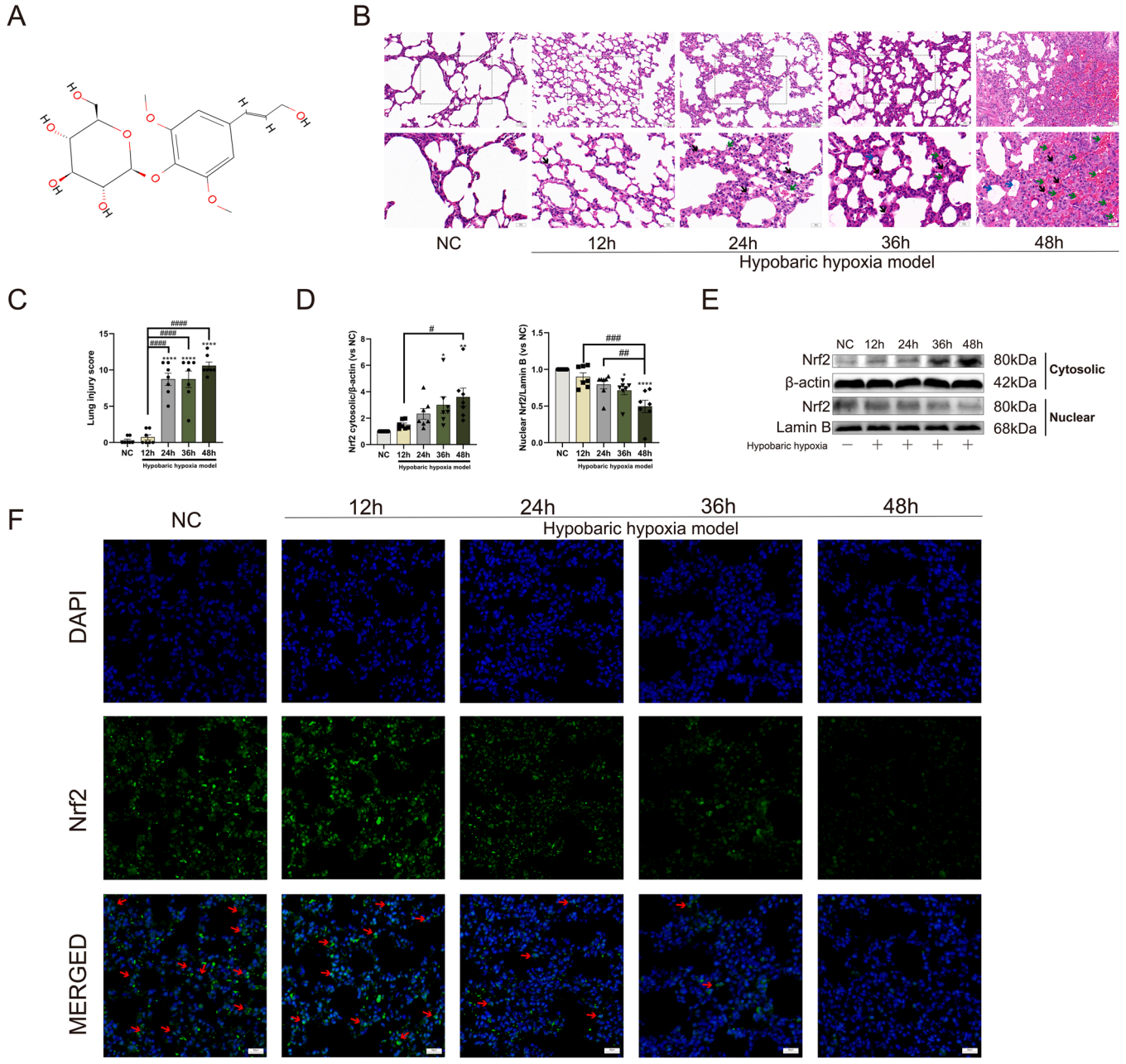

Fig. 1. Hypobaric hypoxia exposure suppressed Nrf2 activation. (A) The chemical structure of eleutheroside B. (B) Lung injury was assessed by H&E staining. Bar = 50 μm, magnification 200 × for the upper row and 400 × for the lower row, n = 4. Black arrows for inflammatory exudate; green arrows for hemorrhage; blue arrows for inflammatory infiltration. (C) Semi-quantitative histopathological score of high-altitude pulmonary edema. (D-E) Western blotting of cytosolic Nrf2 and nuclear Nrf2. (F) Immunofluorescence staining showing Nrf2 nuclear translocation (red arrowheads). Bar = 50 μm, magnification 400 × . The values are expressed as the means ± SEM (n = 7). *$P < 0.05$, **$P < 0.01$, and ****$P < 0.0001$ versus the NC group; #$P < 0.05$, ##$P < 0.01$, ###$P < 0.001$, and ####$P < 0.0001$ versus the 48 h group. NC normoxia control, DAPI 4′− 6-diamidino-2-phenylindole.

2.15. Statistical analysis

Data are expressed as mean and standard error of the mean (SEM). To compare normally distributed data, we used the one-way analysis of variance (ANOVA). The Kruskal-Wallis test was used to compare data which did not meet the normal distribution. Statistical differences were considered significant with a p-value < 0.05. Data were analyzed and plotted with GraphPad Prism 8.0 software (San Diego, CA, USA).

3. Results

3.1. Hypobaric hypoxia inhibited the nuclear translocation of Nrf2

First, the chemical structure of eleutheroside B is shown in Fig. 1A. Regarding the HAPE model in rats, we evaluated different time intervals of hypobaric hypoxia exposure. As shown in Fig. 1B and C, hypobaric hypoxia caused the most serious lung damage at 48 h with edema, alveolar hemorrhage, and inflammatory cell infiltration. A previous report found that Nrf2 activation could effectively alleviate hypoxia-induced ROS production. We demonstrated that hypobaric hypoxia exposure increased the Nrf2 expression in the cytoplasm but decreased the translocation of Nrf2 into the nucleus. Findings were evident after 48 h of hypobaric hypoxia exposure (Fig. 1D and E). Immunofluorescence staining showed a poor translocation ability of Nrf2 at 48 h compared with other time intervals (Fig. 1F). The progression of HAPE might be precipitated by an inhibited translocation of Nrf2 into the nucleus, ultimately resulting in lung damage.

3.2. Eleutheroside B attenuated lung edema

In the phase II of the research, we examined the effects of eleutheroside B on lung edema, inflammatory cytokines, and changes in blood gas indexes. We demonstrated that eleutheroside B reduced the increased W/D ratio after hypobaric hypoxia exposure, suggesting the remission of lung edema (Fig. 2A). As displayed in Fig. 2B and C, the pathological damage of lung tissues was alleviated by eleutheroside B in a dose-dependent manner. The alveolar hemorrhage, inflammatory cell infiltration, and alveolar wall thickening observed in the HHM group were reversed by eleutheroside B.

High altitude hypoxia influences acid-base balance. Analysis of SaO_2, PaO_2, Hct, Hb, pH, $PaCO_2$, and HCO_3 assessed the effects of hypoxia on acid-base balance. We found reduced levels of SaO_2, PaO_2, and HCO_3 and increased levels of pH, Hct and Hb after hypobaric hypoxia exposure. These changes were reversed by eleutheroside B pretreatment. Albeit not statistically significant, $PaCO_2$ levels were slightly increased in the EB 50 and EB 100 groups compared to the HHM group (Fig. 2D).

Previous studies described the total protein content in BALF, a marker of alveolar permeability and severity of pulmonary edema [27]. We found that the total protein content in BALF was significantly augmented after hypobaric hypoxia exposure. Eleutheroside B pretreatment inhibited the occurrence of the phenomenon (Fig. 2E).

Overexpression of VEGF, TNF-α, and IL-1β enhanced vascular permeability and pulmonary edema [28]. We showed that VEGF, TNF-α, and IL-1β contents in BALF were elevated after hypobaric hypoxia exposure. Pretreatment with eleutheroside B blocked any increases in these proteins (Fig. 2F). Eleutheroside B pretreatment regulated acid-base balance and decreased lung edema by reducing total protein content, VEGF, TNF-α, and IL-1β in BALF to resist hypoxia.

3.3. Eleutheroside B facilitated Nrf2 translocation to the nucleus

Based on our findings in vivo, we explored whether eleutheroside B could upregulate Nrf2 expression in the nucleus in HAPE rats. We analyzed the expression levels of cytosolic and nuclear Nrf2 in lung samples of rats. As shown by western blotting, the expression level of cytosolic Nrf2 was significantly elevated by hypobaric hypoxia exposure. Following eleutheroside B pretreatment, the cytosolic Nrf2 level restored to baseline conditions (Fig. 3A and B). In the HHM group, a decreased expression of nuclear Nrf2 was observed. After pretreatment with eleutheroside B, the expression level of nuclear Nrf2 increased in a dose-dependent manner (Fig. 3C and D). These results confirmed that eleutheroside B may facilitate Nrf2 translocation into the nucleus.

3.4. Eleutheroside B alleviated oxidative stress induced by hypobaric hypoxia

To prove the protective mechanisms in vivo of eleutheroside B, we investigated whether eleutheroside B could inhibit hypobaric hypoxia-induced oxidative stress. As shown by flow cytometry and oxidative stress assays, we revealed that eleutheroside B inhibited ROS accumulation in HAPE rats (Fig. 4A and B). The levels of 4-HNE and MDA were diminished while the CAT levels were elevated after eleutheroside B pretreatment (Fig. 4C). These findings indicated the protective effects of eleutheroside B in HAPE rats.

3.5. Eleutheroside B suppressed ferroptosis in HAPE rats

We detected iron levels in lung tissues and observed lung tissues by TEM to determine any ferroptosis-related lung damage. In the HHM group, the iron levels in lung tissues increased after hypobaric hypoxia exposure (Fig. 5A). Changes in mitochondrial morphology, a distinctive feature of ferroptosis, were observed in type 2 alveolar epithelial cells by TEM. Ferroptosis is usually characterized by the disruption of the mitochondria cristae, reduced mitochondrial volume, augmented mitochondrial electron density, and membrane density [29]. As shown in Fig. 5B, the mitochondrial alterations were reversed by eleutheroside B pretreatment. The levels of several proteins involved in ferroptosis including SLC7A11, GPX4, HO-1, TFRC, FTH1, NOX1, and COX2 were examined using western blotting. As shown in Fig. 5C and D, the expression of SLC7A11, FTH1, GPX4, and HO-1 was decreased in the HHM group. Additionally, the expression of TFRC, NOX1, and COX2 was increased in the HHM group. The aforementioned changes of ferroptosis-related proteins were inhibited by eleutheroside B administration. Consistent with western blotting results, GPX4 levels were increased by eleutheroside B pretreatment when observed by immunofluorescence staining (Fig. 5E and F).

3.6. Eleutheroside B inhibited necroptosis in lung tissues of HAPE rats

Several necroptosis-related proteins were evaluated using western blotting. As illustrated in Fig. 6A and B, we showed higher levels of RIPK1, RIPK3 and phospho-MLKL in the HHM group. In addition, the expression of RIPK1, RIPK3, and phospho-MLKL declined in the EB 50 and EB100 groups. When observed by immunofluorescence staining, the levels of RIPK3 were increased by eleutheroside B pretreatment (Fig. 6C and D).

3.7. Eleutheroside B attenuated HAPE through inhibition of oxidative stress via promoting Nrf2 nuclear translocation

We explored the specific mechanisms of Nrf2 in HAPE rats. ML385, an inhibitor of Nrf2, was applied during the phase III of the research. H&E staining revealed that ML385 administration abolished the therapeutic effects of eleutheroside B in the EB100 + mL 385 group, showing severe alveolar hemorrhage and inflammatory cell infiltration (Fig. 7A and B). Consistent findings were observed evaluating the W/D ratio (Fig. 7C). Western blotting findings suggested that ML385 reversed the increased nuclear translocation of Nrf2 induced by eleutheroside B. The expression of nuclear and cytoplasmic Nrf2 was inhibited in the EB100 + ML385 group compared to the EB100 group (Fig. 7D and E). ML385 inhibited the effects of eleutheroside B on intracellular ROS production in HAPE rats (Fig. 7F and G). These findings revealed that the

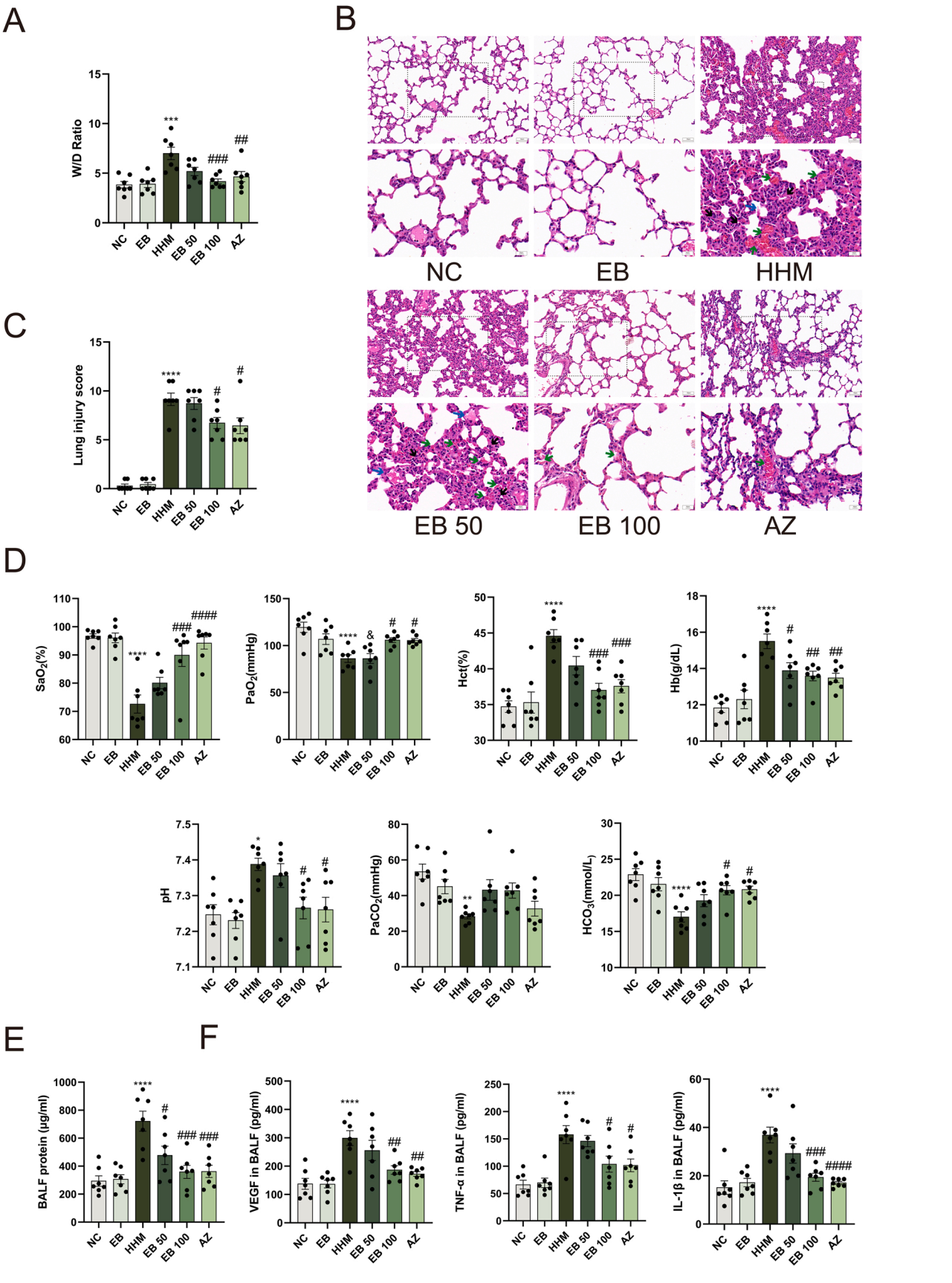

(caption on next page)

Fig. 2. The protective effects of eleutheroside B pretreatment in HAPE. (A) Effect of eleutheroside B pretreatment on lung wet/dry (W/D) ratio. (B) Lung injury was assessed by H&E staining. Bar = 50 μm, magnification 200 × for the upper row and 400 × for the lower row, n = 4. Black arrows for inflammatory exudate; green arrows for hemorrhage; blue arrows for inflammatory infiltration. (C) Semi-quantitative histopathological score of HAPE. (D) Effect of eleutheroside B on SaO2, PaO2, Hct, Hb, pH, PaCO2, and HCO3 in HAPE. (E) Effect of eleutheroside B pretreatment on total protein in BALF. (F) Effect of eleutheroside B on VEGF, TNF-α, and IL-1β in BALF. The values are expressed as the means ± SEM (n = 7). *$P < 0.05$, **$P < 0.01$, ***$P < 0.001$, and ****$P < 0.0001$ versus the NC group; #$P < 0.05$, ##$P < 0.01$, ###$P < 0.001$, and ####$P < 0.0001$ versus the HHM group. NC normoxia control, HHM hypobaric hypoxia model, EB eleutheroside B (100 mg/kg) alone, EB 50 eleutheroside B (50 mg/kg) before hypobaric hypoxia exposure, EB 100 eleutheroside B (100 mg/kg) before hypobaric hypoxia exposure, AZ acetazolamide (50 mg/Kg) before hypobaric hypoxia exposure, W/D wet-to-dry, BALF bronchoalveolar lavage fluid, VEGF vascular endothelial growth factor, TNF-α tumor necrosis factor-α, IL-6 interleukin-6.

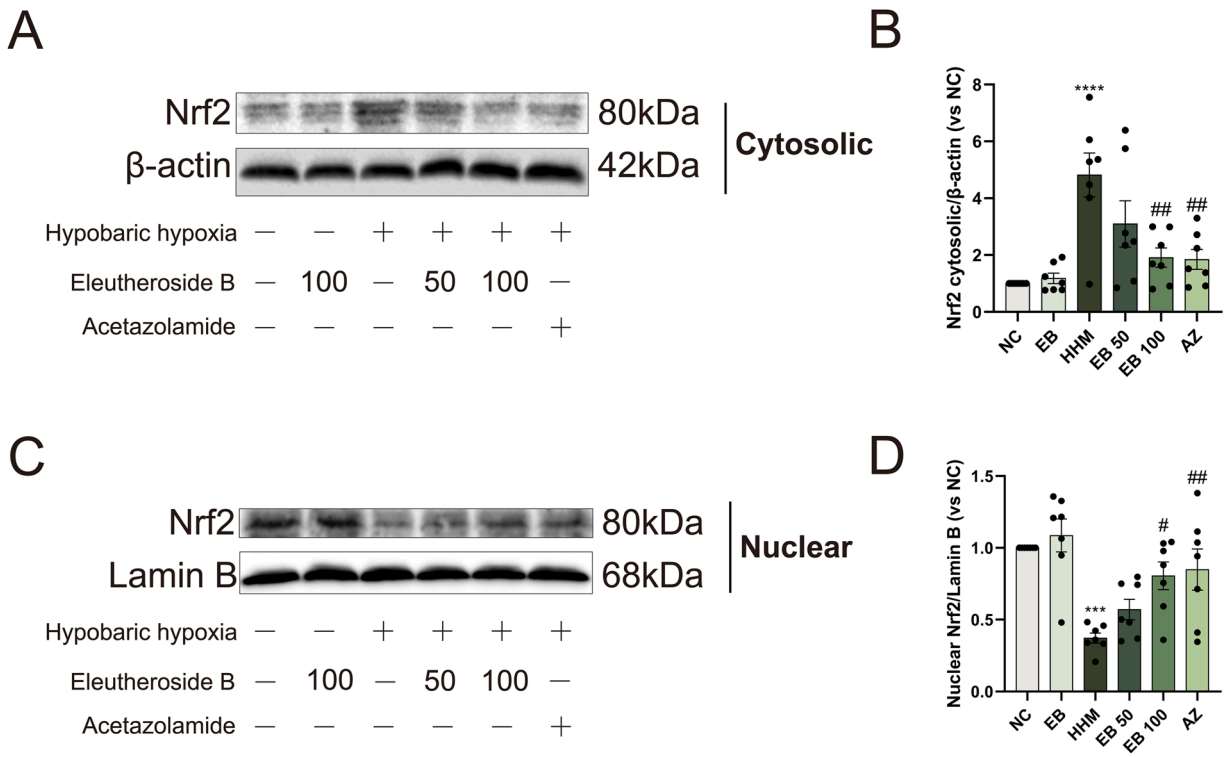

Fig. 3. Eleutheroside B pretreatment increased Nrf2 activation. (A-B) Western blotting of cytosolic Nrf2. (C-D) Western blotting of nuclear Nrf2. The values are expressed as the means ± SEM (n = 7). ***$P < 0.001$ and ****$P < 0.0001$ versus the NC group; #$P < 0.05$ and ##$P < 0.01$ versus the HHM group. NC normoxia control, HHM hypobaric hypoxia model, EB eleutheroside B (100 mg/kg) alone, EB 50 eleutheroside B (50 mg/kg) before hypobaric hypoxia exposure, EB 100 eleutheroside B (100 mg/kg) before hypobaric hypoxia exposure, AZ acetazolamide (50 mg/Kg) before hypobaric hypoxia exposure.

nuclear translocation of Nrf2 played an essential role against HAPE. Eleutheroside B might be a beneficial treatment against HAPE by activating Nrf2 translocation.

3.8. Inhibition of Nrf2 eliminated anti-ferroptosis effects of eleutheroside B

We explored whether inhibition of Nrf2 affected ferroptosis after hypobaric hypoxia exposure. Western blotting results found that ML385 suppressed the upregulation of SLC7A11, FTH1, GPX4, and HO-1 by eleutheroside B. In addition, ML385 inhibited the downregulation of TFRC, NOX1, and COX2 by eleutheroside B (Fig. 8A and B). In comparison with the EB100 group, TEM results indicated that the ferroptosis-associated alterations of type 2 alveolar epithelial cells were aggravated in the EB100 + ML385 group, displaying a more severe disruption of the mitochondria cristae and reduced mitochondrial volume (Fig. 8C). Consistent with western blotting results, immunofluorescence staining found a lower expression of GPX4 in the EB100 + ML385 group compared with the EB100 group (Fig. 8D and E). These findings demonstrated that eleutheroside B could alleviate HAPE by activating the nuclear translocation of Nrf2 and suppressing ferroptosis.

3.9. Eleutheroside B reduced necroptosis by facilitating the nuclear translocation of Nrf2

To further investigate the role of Nrf2 during necroptosis in HAPE rats, we detected necroptosis-related proteins using western blotting. As shown in Fig. 9A and B, ML385 abolished the downregulation of RIPK1, RIPK3 and p-MLKL induced by eleutheroside B. Additionally, immunofluorescence staining found an increased expression of RIPK3 after ML385 treatment in the EB100 + ML385 group (Fig. 9D and E). These results suggested that the deletion of Nrf2 reduced the anti-necroptosis effects induced by eleutheroside B treatment.

4. Discussion

In the current study, we investigated the potential therapeutic effects of eleutheroside B against HAPE. We found that eleutheroside B inhibited oxidative stress, ferroptosis, and necroptosis by activating the nuclear translocation of Nrf2. These findings were validated by the experimental implementation of ML385, a Nrf2 inhibitor. A schematic presentation of these potential therapeutic effects is presented in Fig. 10.

HAPE is a noncardiogenic pulmonary edema with a normal pulmonary capillary wedge pressure [30]. It is characterized by hypoxic pulmonary hypertension, increased permeability of the alveolocapillary

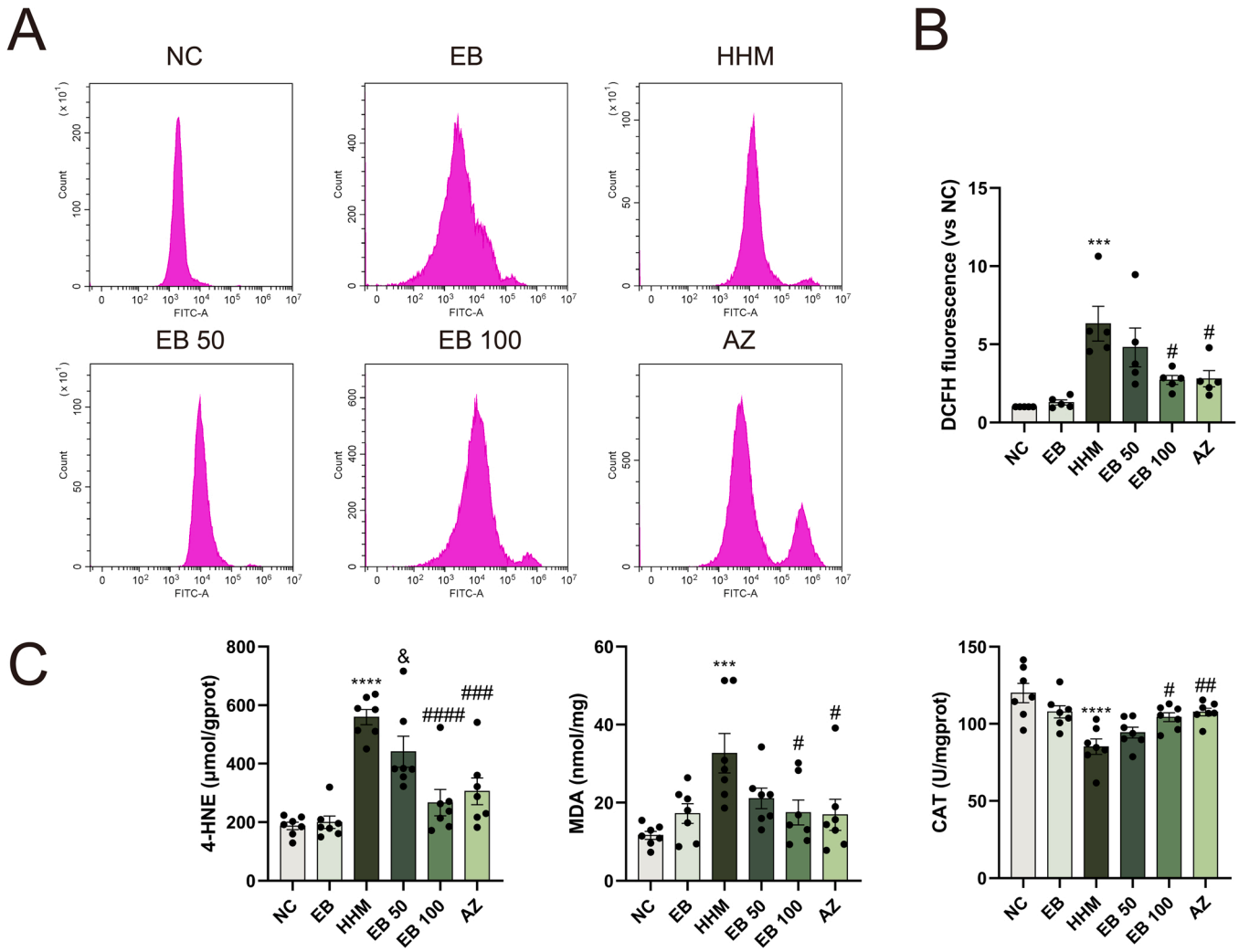

Fig. 4. Eleutheroside B pretreatment inhibited oxidative stress. (A-B) Effect of eleutheroside B on intracellular ROS levels. (C) Effect of eleutheroside B on 4-HNE, MDA, and CAT in lung tissues. The values are expressed as the means ± SEM (n = 7). ***P < 0.001 and ****P < 0.0001 versus the NC group; *#P* < 0.05, *##P* < 0.01, *###P* < 0.001, and *####P* < 0.0001 versus the HHM group; *&P* < 0.05 versus the EB 100 group. NC normoxia control, HHM hypobaric hypoxia model, EB eleutheroside B (100 mg/kg) alone, EB 50 eleutheroside B (50 mg/kg) before hypobaric hypoxia exposure, EB 100 eleutheroside B (100 mg/kg) before hypobaric hypoxia exposure, AZ acetazolamide (50 mg/Kg) before hypobaric hypoxia exposure. DCFH dichlorodihydrofluorescein diacetate, 4-HNE 4-hydroxynonenal, MDA malondialdehyde, CAT catalase.

membrane, and alveolar congestion [2]. Pharmacotherapy of HAPE includes glucocorticosteroids, pulmonary vasodilators, and carbonic anhydrase inhibitors. Considering that the mentioned pharmacotherapy has many serious side effects, the search for novel therapeutic strategies is urgent [31–33]. Consistent with a previously published study [34], we observed an elevated total protein content in BALF after hypobaric hypoxia exposure. VEGF, a potent angiogenic factor, increases endothelial permeability and can cause pulmonary edema [35]. IL-1β and TNF-α are pro-inflammatory factors that are promptly released in the presence of lung edema [36,37]. In this study, hypobaric hypoxia exposure markedly elevated VEGF, IL-1β, and TNF-α levels.

Progression of HAPE is rapid and associated with high mortality. Acid-base disorders are commonly seen during HAPE [38]. Consistent with a previous study in vivo [39], we observed lower levels of PaO_2 and $PaCO_2$. The observed findings may result from hyperventilation and hypocapnia induced by hypobaric hypoxia. Although it did not show any statistical significance between the EB 100 group and the HHM group in the PaCO2 level, an increasing trend with EB 100 groups was apparent. It might be due to the PaCO2 indicator being very sensitive and presenting a quick response to variations in the hypobaric hypoxia conditions. PaCO2 detection must be proceed as rapidly as can be accomplished after removing from cabin. An increase in hemoglobin concentration can augment the capacity of blood to transport oxygen, providing a better oxygen delivery to peripheral tissues [40]. Consistent with previously published research [39], we observed that hemoglobin and hematocrit were increased after hypobaric hypoxia exposure.

The Nrf2 activation mitigated ROS accumulation and vascular leakage caused by high altitude [9]. Prophylactic medications for high altitude illness may be sufficient to protect lung function. Eleutheroside B, a compound isolated from Acanthopanax senticosus, can improve the nuclear translocation of Nrf2 and restore the cellular redox balance [41]. We found that eleutheroside B pretreatment protected from HAPE by facilitating Nrf2 activation and therefore promoting antioxidant activities. In accordance with histopathology and western blotting results, we selected 48 h of hypobaric hypoxia exposure to produce the HAPE model in rats. After 48 h of modeling, the expression of Nrf2 reduced in the nucleus and increased in the cytoplasm of the HHM group. These findings were consistent with the study of *Zhang* et al. [42], where hypoxia significantly suppressed the expression of nuclear Nrf2. Nuclear Nrf2 has, however, been described at high levels in another study [43]. This controversy may partly originate from different hypoxia exposures, Nrf2 metabolism, or cell heterogeneity. We elucidated that the

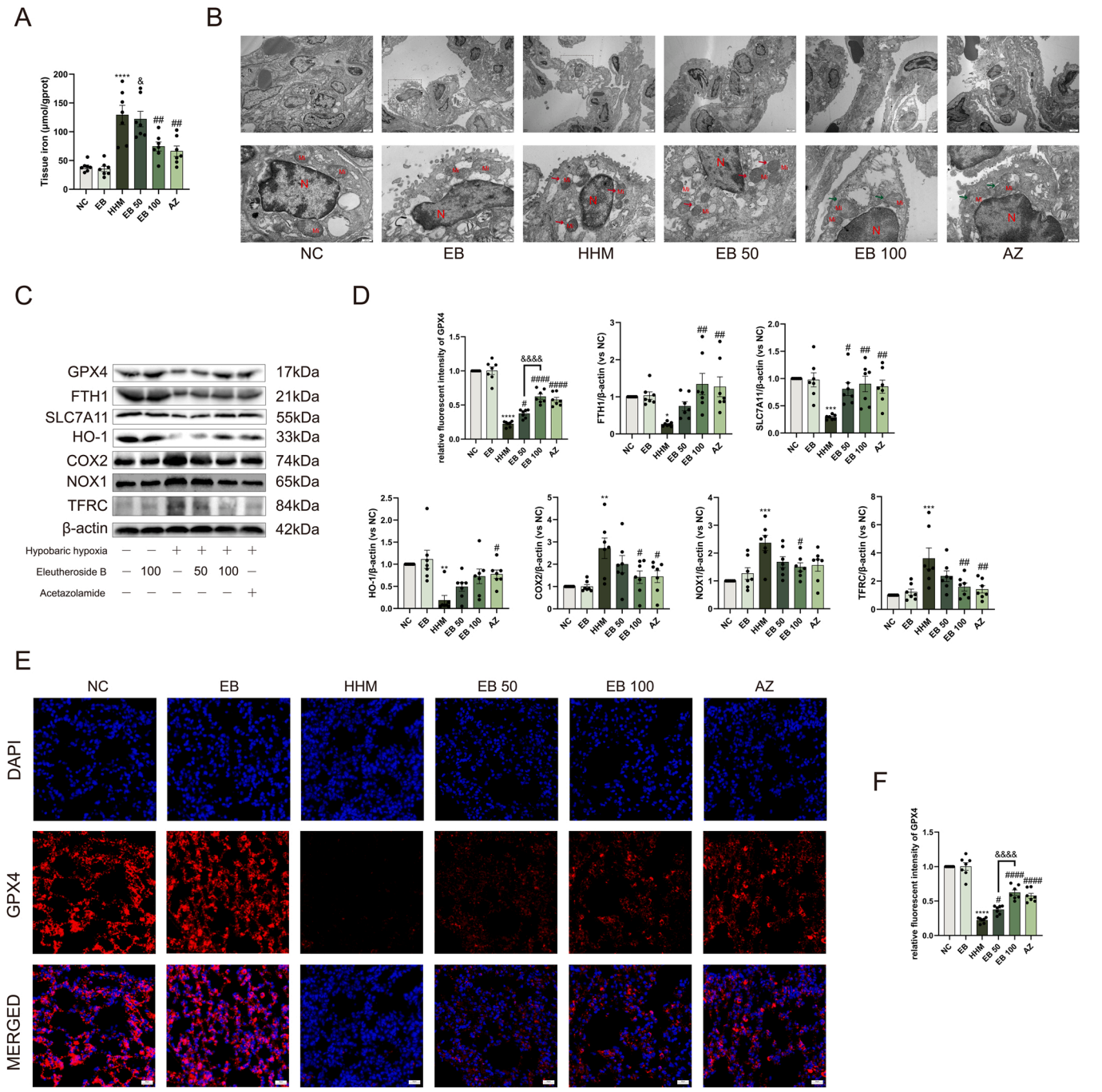

Fig. 5. The anti-ferroptosis effects of eleutheroside B pretreatment in HAPE. (A) Effect of eleutheroside B on tissue iron. (B) TEM was utilized to visualize mitochondrial changes of ferroptosis in type II alveolar epithelial cells (mitochondria, Mi; nuclear, N). Bar = 2 μm, magnification 6000 × for the upper row and 25,000× for the lower row, n = 4. Red arrows for decreased mitochondrial cristae and increased mitochondrial electron density in ferroptosis; green arrows for mitochondrial swelling. (C-D) Western blotting analysis of GPX4, FTH1, SLC7A11, HO-1, COX2, NOX1, and TFRC. (E) Immunofluorescence staining of GPX4 in lung tissues. Bar = 50 μm, magnification 400×. (F) The relative fluorescent intensity of GPX4 in lung tissues. The values are expressed as the means ± SEM (n = 7). $^{*}P < 0.05$, $^{**}P < 0.01$, $^{***}P < 0.001$, and $^{****}P < 0.0001$ versus the NC group; $\#P < 0.05$, $\#\#P < 0.01$, and $\#\#\#\#P < 0.0001$ versus the HHM group; $\&P < 0.05$ and $\&\&\&\&P < 0.0001$ versus the EB 100 group. NC normoxia control, HHM hypobaric hypoxia model, EB eleutheroside B (100 mg/kg) alone, EB 50 eleutheroside B (50 mg/kg) before hypobaric hypoxia exposure, EB 100 eleutheroside B (100 mg/kg) before hypobaric hypoxia exposure, AZ acetazolamide (50 mg/Kg) before hypobaric hypoxia exposure, DAPI 4′− 6-diamidino-2-phenylindole.

transcriptional activation of Nrf2 changed in a time-dependent manner, affecting the progression of HAPE.

Previous studies found an excessive ROS production in HAPE [7]. As the primary organelle damaged by ferroptosis, mitochondria are a main source of ROS and also a target of ROS [44]. The reactions of the TCA cycle occur inside mitochondria, followed by the occurrence of oxidative phosphorylation and electron transfer chain (ETC). Meanwhile, mitochondria are important sites of intracellular ROS production and elimination [10]. The destruction of mitochondria could trigger ROS accumulation, which induces causes mitochondrial dysfunction [45]. A recent study showed that eleutheroside B was used as a selective COX2 inhibitor, exerting anti-inflammatory effects [46]. When eleutheroside B was used for pretreatment, nuclear Nrf2 significantly increased in parallel to a reduction of lung edema and ROS production. These results

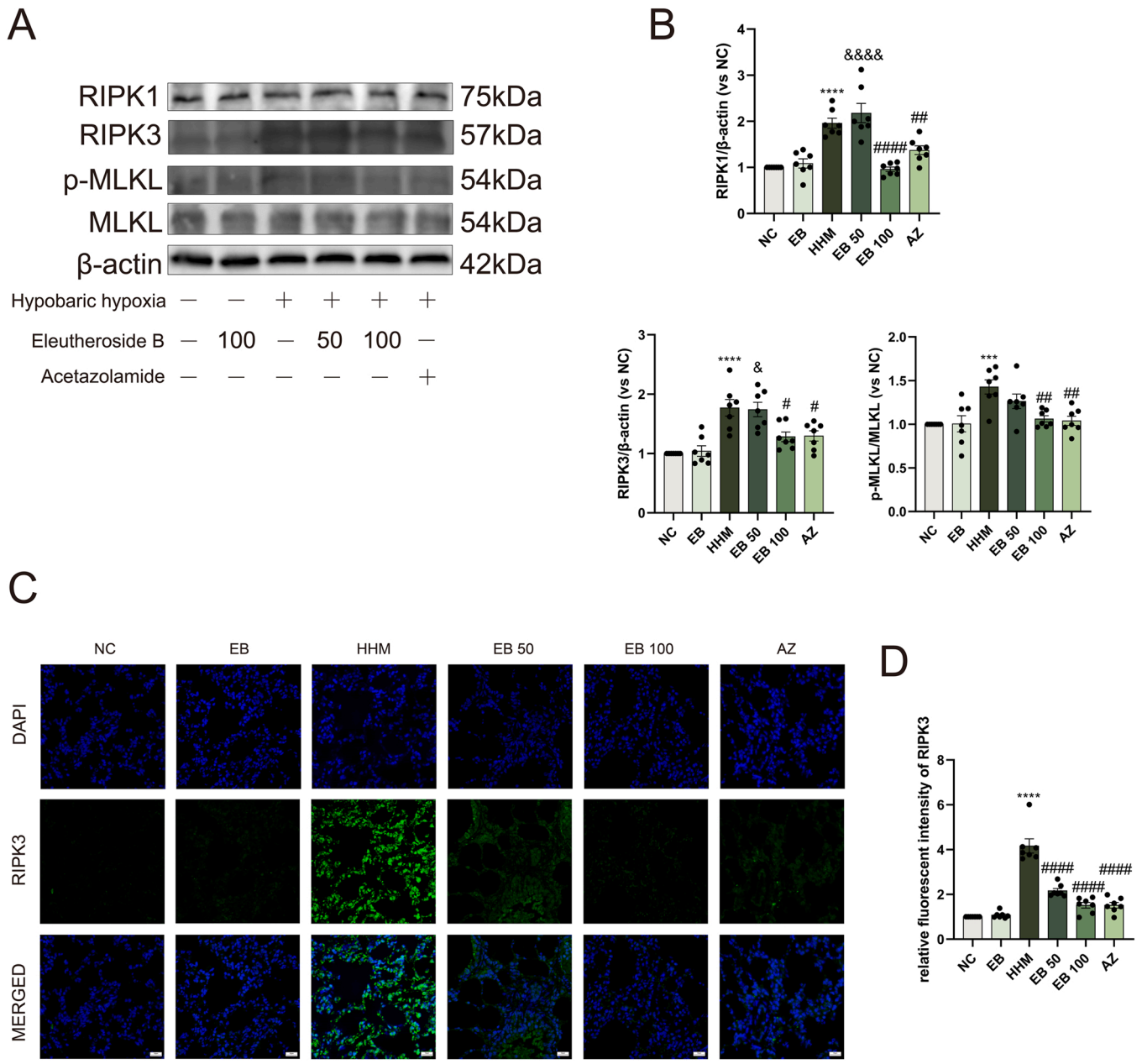

Fig. 6. The anti-necroptosis effects of eleutheroside B pretreatment in HAPE. (A-B) Western blotting analysis of RIPK1, RIPK3, and p-MLKL. (C) Immunofluorescence staining of RIPK3 in lung tissues. Bar = 50 μm, magnification 400 × . (D) The relative fluorescent intensity of RIPK3 in lung tissues. The values are expressed as the means ± SEM (n = 7). ***$P < 0.001$ and ****$P < 0.0001$ versus the NC group; #$P < 0.05$, ##$P < 0.01$, and ####$P < 0.0001$ versus the HHM group; &$P < 0.05$ and &&&&$P < 0.0001$ versus the EB 100 group. NC normoxia control, HHM hypobaric hypoxia model, EB eleutheroside B (100 mg/kg) alone, EB 50 eleutheroside B (50 mg/kg) before hypobaric hypoxia exposure, EB 100 eleutheroside B (100 mg/kg) before hypobaric hypoxia exposure, AZ acetazolamide (50 mg/Kg) before hypobaric hypoxia exposure, DAPI 4′− 6-diamidino-2-phenylindole.

may explain the antioxidant effects of eleutheroside B. We evaluated several oxidative stress-related indicators, including MDA, CAT, and 4-HNE. Lipid peroxidation was associated with elevated MDA, and 4-HNE, while the antioxidant enzyme CAT was decreased [47,48]. The aforementioned alterations were reversed by eleutheroside B pretreatment.

Ferroptosis is a form of programmed cell death characterized by iron-dependent lipid peroxidation. Ferroptosis was observed in neuronal cells during acute mountain sickness, contributing to brain damage [11]. Excessive free iron, lipid peroxidation, and inhibition of Nrf2 are key processes during cellular ferroptosis. Several studies described that the transcriptional activation of Nrf2 contributed to ferroptosis resistance through the upregulation of genes involved in iron and ROS metabolism [49,50]. In this research, we observed higher levels of TFRC, COX2, and NOX1 along with lower expression levels of SLC7A11, FTH1, GPX4, and HO-1 in the HHM group. COX2 and NOX1 are commonly used as indicators for ferroptosis because they mediate plasma membrane lipid peroxidation and ferroptosis [51,52]. A recent study found that the inhibition of nuclear Nrf2 suppressed GPX4 transcription, resulting in more ferroptosis in cardiomyoblasts [53]. HO-1 and SLC7A11 have been previously involved in Nrf2-mediated protection of ferroptosis [54,55]. HO-1 is a major ARE-inducible antioxidant enzyme that mediates the heme degradation of heme into ferrous iron, carbon monoxide (CO), and biliverdin [56]. Nrf2 binds to antioxidant response elements and activates the transcription of HO-1 to counteract ROS. In vitro and in vivo experiments confirmed that Nrf2/HO-1 pathway activation could

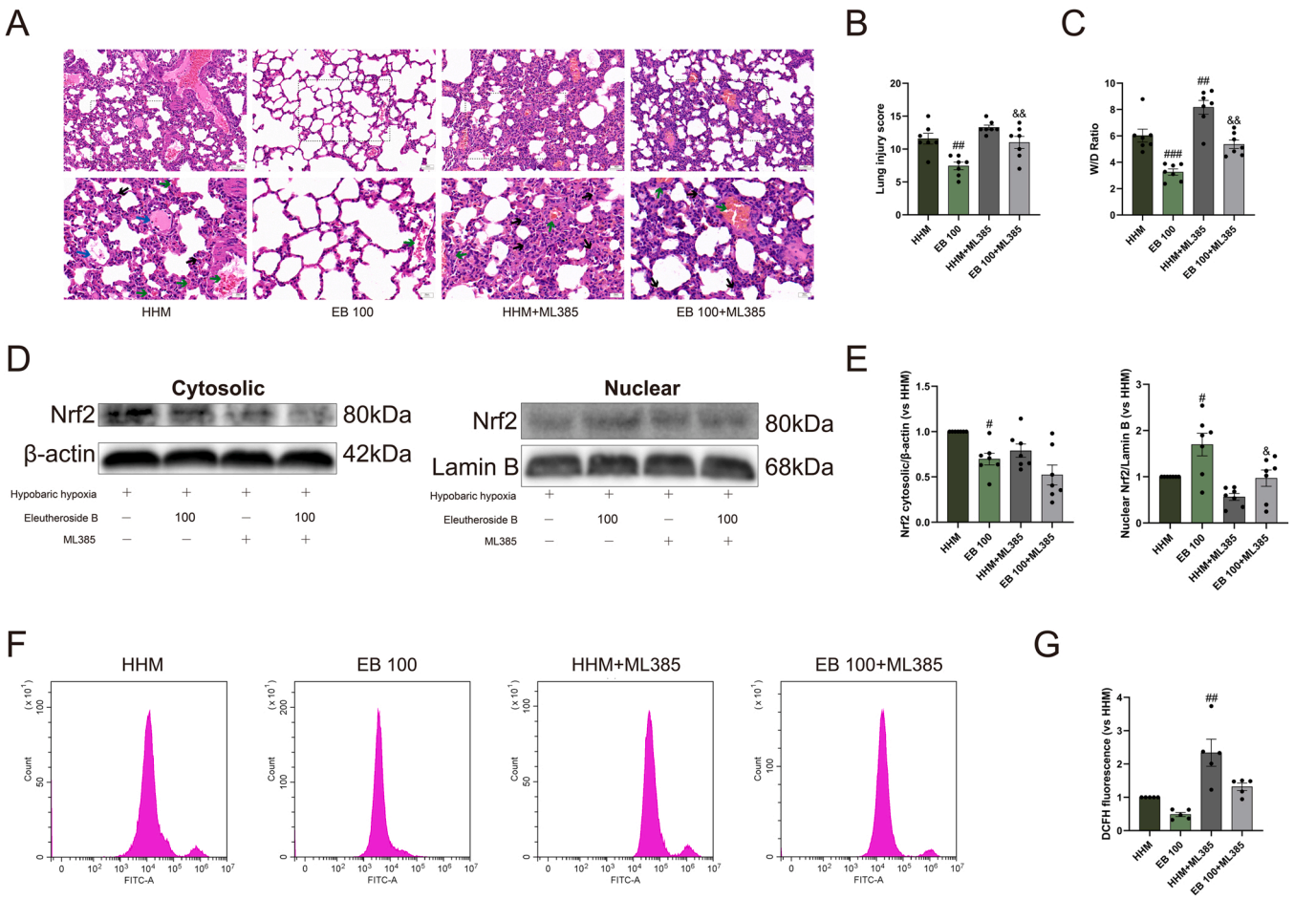

Fig. 7. Nrf2 inhibition diminished the effects of Eleutheroside B pretreatment. (A) Lung injury was assessed by H&E staining. Bar = 50 μm, magnification 200 × for the upper row and 400 × for the lower row, n = 4. Black arrows for inflammatory exudate; green arrows for hemorrhage; blue arrows for inflammatory infiltration. (B) Semi-quantitative histopathological score. (C) Effect of ML385 on lung wet/dry (W/D) ratio. (D-E) Effect of ML385 on Nrf2 translocation. (F-G) Effect of ML385 on intracellular ROS levels. The values are expressed as the means ± SEM (n = 7). #$P < 0.05$, ##$P < 0.01$, and ###$P < 0.001$ versus the HHM group; &$P < 0.05$ and &&$P < 0.01$ versus the EB 100 group. HHM hypobaric hypoxia model, EB 100 eleutheroside B (100 mg/kg) before hypobaric hypoxia exposure, HHM+ML385 ML385 (30 mg/Kg) before hypobaric hypoxia exposure, EB100 +ML385 eleutheroside B (100 mg/kg) and ML385 (30 mg/Kg) before hypobaric hypoxia exposure, W/D wet-to-dry, DCFH dichlorodihydrofluorescein diacetate.

alleviate liver injury by inhibiting ferroptosis [57]. Moreover, Nrf2 activation could increase HO-1 expression, contributing to suppressing oxidative stress in lung injury [58]. Chemical and genetic inhibition of TFRC diminished ferroptotic cell death, thereby mitigating acute liver injury [59]. Our results suggested that the potential therapeutic effects of eleutheroside B may be mediated via Nrf2 upregulation. ML385, an Nrf2 inhibitor, abolished the beneficial effects of eleutheroside B in HAPE rats, suggesting that ferroptosis might be a relevant pathological process during HAPE.

Necroptosis is an alternative form of programmed cell death regulated by RIPK1 and RIPK3 [60]. A previous study demonstrated the presence of necroptosis in hypoxia-induced disease conditions [14]. The anti-necroptosis effects of eleutheroside B were also reported in a more recent study, where eleutheroside B attenuated acute kidney injury by inhibiting apoptosis and necroptosis via the nuclear factor-κB (NF-κB) signaling pathway [20]. Consistent with previous findings, we found that eleutheroside B suppressed necroptosis in HAPE rats. An in vitro study found that gallic acid improved ethanol-induced hepatocyte necroptosis [61], suggesting that Nrf2 activation is essential for its anti-necroptosis effects. In our study, eleutheroside B reversed the decreased activity of Nrf2 induced by hypobaric hypoxia. When ML385 was administered, the expression of necroptosis-related proteins was upregulated.

Intracellular ROS production has been implicated in the development of ferroptosis and necroptosis [62–64]. However, the mechanisms underlying the relationship among ROS production, ferroptosis, and necroptosis remain unclear. Previous studies elucidated that ROS promoted RIPK1 autophosphorylation, recruiting RIPK3 to form a necrosome and mediating necroptosis [65]. Nrf2 triggered the expression of ROS-detoxifying enzymes, weakening ROS accumulation. We speculated that HAPE might be alleviated by activating Nrf2, which in turn decreased ROS production, then ferroptosis and necroptosis.

Our results implicated that eleutheroside B could become a promising preparation for the clinical treatment of HAPE. The initial dose of eleutheroside B in entry into man studies is 86.4 mg (for a 60 kg human) and the conversion of human clinical dosage is referred to a previous study [66]. In the future, the clinical application of eleutheroside B needs a strictly designed RCT study and must be interpreted in conjunction with the clinical presentation, clinical pharmacology, pharmacokinetics, and pharmaceutics.

The present study, for the first time, demonstrates the effects of eleutheroside B treatment in HAPE in vivo. Given the efficacy and safety of eleutheroside B, it is expected to be a candidate for the treatment of HAPE, with the purpose of a multi-target therapy. These results are relevant for the future direction of research and clinical application. In addition, anti-ferroptosis and anti-necroptosis drugs could also be used as tools to gain deeper insights into HAPE pathogenesis and drug therapy.

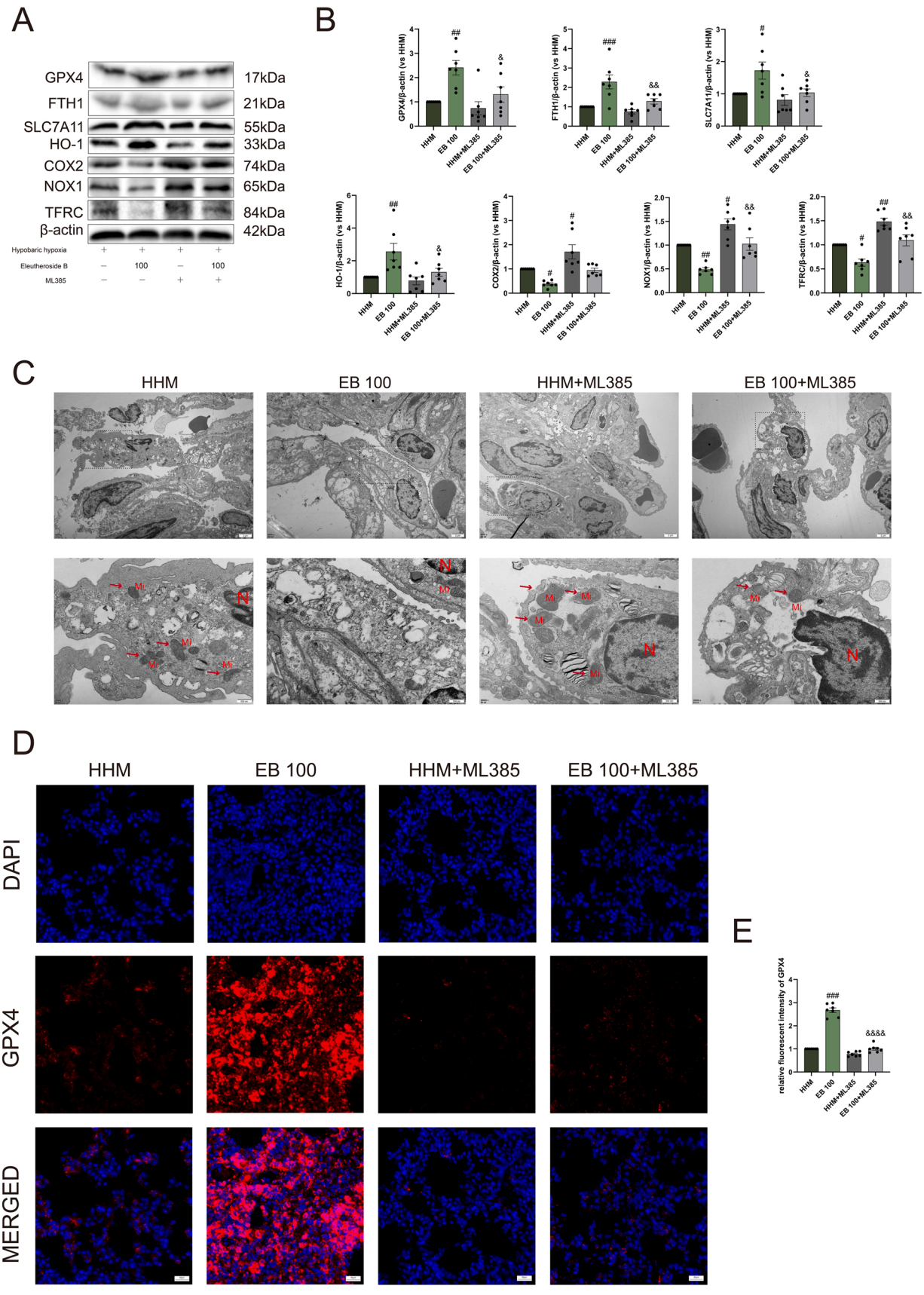

(caption on next page)

Fig. 8. ML385 eliminated anti-ferroptosis effects of eleutheroside B. (A-B) Western blotting analysis of GPX4, FTH1, SLC7A11, HO-1, COX2, NOX1, and TFRC. (C) TEM was utilized to visualize mitochondrial changes of ferroptosis in type II alveolar epithelial cells (mitochondria, Mi; nuclear, N). Bar = 2 μm, magnification 6000× for the upper row and 25,000× for the lower row, n = 4. Red arrows for decreased mitochondrial cristae and increased mitochondrial electron density in ferroptosis; green arrows for mitochondrial swelling. (D) Immunofluorescence staining of GPX4 in lung tissues. Bar = 50 μm, magnification 400 × . (E) The relative fluorescent intensity of GPX4 in lung tissues. The values are expressed as the means ± SEM (n = 7). #$P < 0.05$, ##$P < 0.01$, and ###$P < 0.001$ versus the HHM group; &$P < 0.05$, &&$P < 0.01$, and &&&&$P < 0.0001$ versus the EB 100 group. HHM hypobaric hypoxia model, EB 100 eleutheroside B (100 mg/kg) before hypobaric hypoxia exposure, HHM+ML385 ML385 (30 mg/Kg) before hypobaric hypoxia exposure, EB100 +ML385 eleutheroside B (100 mg/kg) and ML385 (30 mg/Kg) before hypobaric hypoxia exposure, DAPI 4′− 6-diamidino-2-phenylindole.

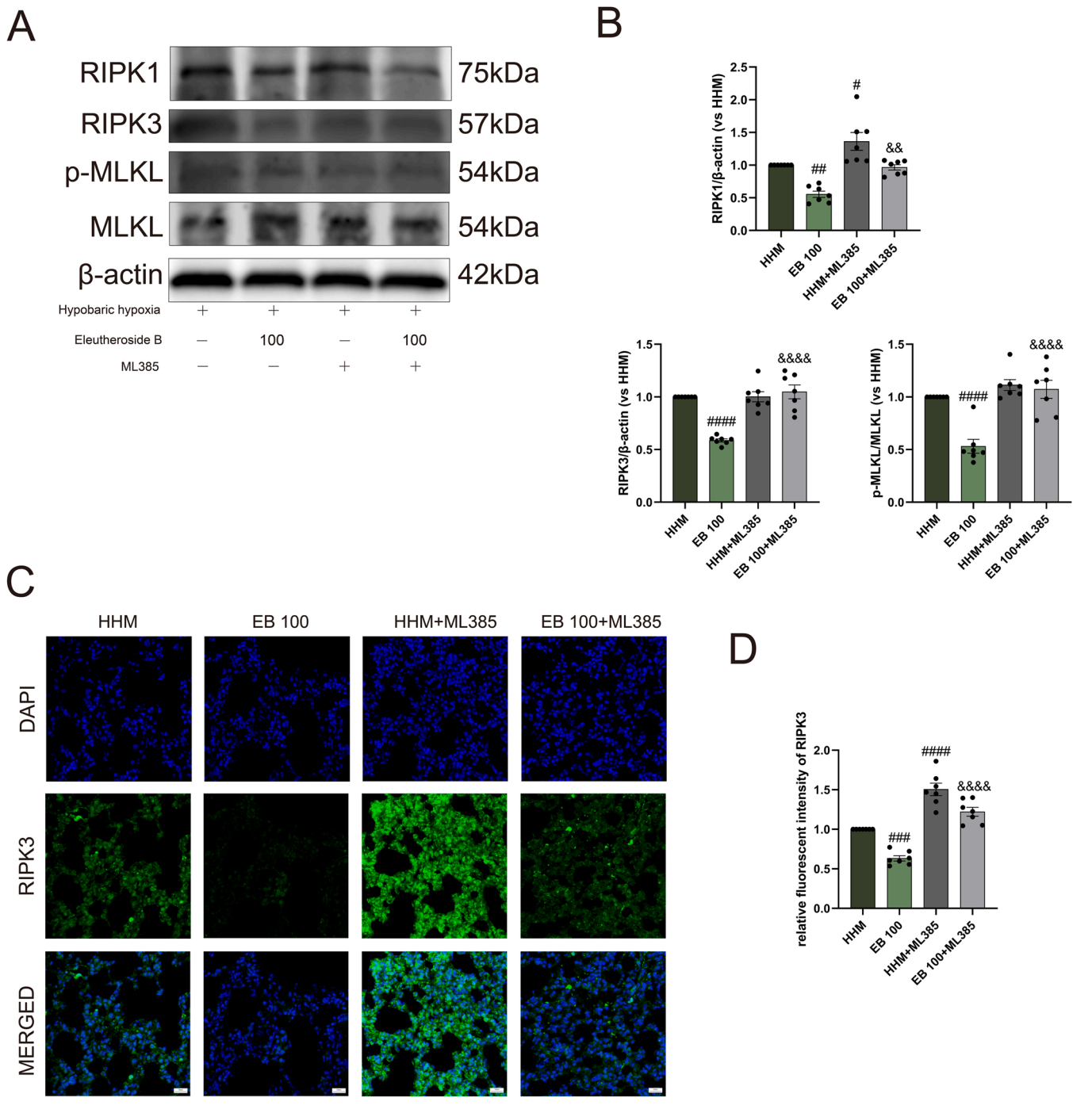

Fig. 9. ML385 abolished anti-necroptosis effects of eleutheroside B. (A-B) Western blotting analysis of RIPK1, RIPK3, and p-MLKL. (C) Immunofluorescence staining of RIPK3 in lung tissues. Bar = 50 μm, magnification 400 × . (D) The relative fluorescent intensity of RIPK3 in lung tissues. The values are expressed as the means ± SEM (n = 7). #$P < 0.05$, ##$P < 0.01$, and ####$P < 0.0001$ versus the HHM group; &&$P < 0.01$ and &&&&$P < 0.0001$ versus the EB 100 group. HHM hypobaric hypoxia model, EB 100 eleutheroside B (100 mg/kg) before hypobaric hypoxia exposure, HHM+ML385 ML385 (30 mg/Kg) before hypobaric hypoxia exposure, EB100 +ML385 eleutheroside B (100 mg/kg) and ML385 (30 mg/Kg) before hypobaric hypoxia exposure, DAPI 4′− 6-diamidino-2-phenylindole.

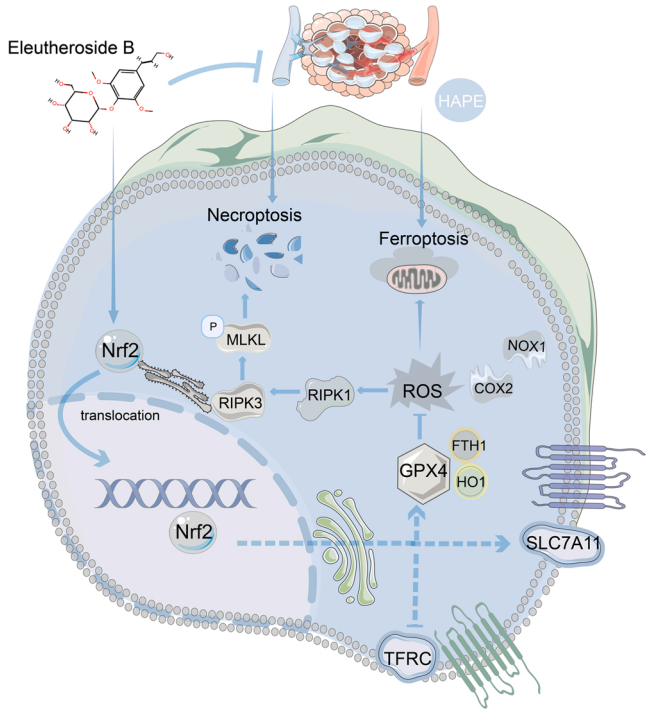

Fig. 10. Eleutheroside B exerts therapeutic effects on HAPE through anti-ferroptosis and anti-necroptosis via Nrf2 activation and ROS inhibition. HPAE, high altitude pulmonary edema.

5. Conclusion

Eleutheroside B pretreatment played a protective role against HAPE by activating Nrf2, alleviating oxidative stress, and reducing ferroptosis and necroptosis. These results were achieved by activating the Nrf2 signaling pathway. The present study emphasized the use of eleutheroside B as a new approach to prevent HAPE and lung edema. In future research, agonizts and inhibitors of ferroptosis and necroptosis would be applied to further explore the specific mechanisms of ferroptosis and necroptosis in HAPE. Further studies should validate the connection and crosstalk between ferroptosis and necroptosis in HAPE.

CRediT authorship contribution statement

Yilan Wang: Conceptualization, Data curation, Formal analysis, Investigation, Methodology, Writing-original draft, Writing-review & editing. **Zherui Shen:** Formal analysis, Investigation, Methodology, Writing-original draft. **Caixia Pei**: Data curation, Investigation. **Sijing Zhao**: Data curation, Investigation. **Nan Jia**: Data curation, Investigation. **Demei Huang**: Software, Methodology. **Xiaomin Wang:** Software, Methodology. **Yongcan Wu**: Software, Methodology. **Shihua Shi**: Validation. **Yacong He:** Formal analysis, Writing-review & editing. **Zhenxing Wang:** Conceptualization, Funding acquisition, Project administration, Resources, Supervision, Writing-review & editing.

Declaration of Competing Interest

The authors declare no conflict of interest.

Acknowledgment

This study was financially supported by National Natural Science Foundation of China (No. 82205043) and China Postdoctoral Science Foundation (No. 2022M710500 and No. YJ20220058). The funder was not involved in the design of the study, nor were they engaged in collection, management, analysis, data-interpretation, report-writing, or the decision to submit the report for publication.

References

[1] A.M. Luks, P.S. Auerbach, L. Freer, C.K. Grissom, L.E. Keyes, S.E. McIntosh, G. W. Rodway, R.B. Schoene, K. Zafren, P.H. Hackett, Wilderness medical society clinical practice guidelines for the prevention and treatment of acute altitude illness: 2019 update, Wilderness Environ. Med. 30 (2019) S3–s18, https://doi.org/10.1016/j.wem.2019.04.006.
[2] P. Woods, J. Alcock, High-altitude pulmonary edema, Evol. Med. Public. Health 9 (2021) 118–119, https://doi.org/10.1093/emph/eoaa052.
[3] A.M. Sophocles Jr., High-altitude pulmonary edema in vail, colorado, 1975-1982, West. J. Med. 144 (1986) 569–573.
[4] T.Y. Wu, S.Q. Ding, J.L. Liu, M.T. Yu, J.H. Jia, Z.C. Chai, R.C. Dai, S.L. Zhang, B. Y. Li, L. Pan, B.Z. Liang, J.Z. Zhao, T. Qi de, Y.F. Sun, B. Kayser, Who should not go high: chronic disease and work at altitude during construction of the qinghai-tibet railroad, High. Alt. Med. Biol. 8 (2007) 88–107, https://doi.org/10.1089/ham.2007.1015.
[5] C. Davis, P. Hackett, Advances in the prevention and treatment of high altitude illness, Emerg. Med. Clin. North Am. 35 (2017) 241–260, https://doi.org/10.1016/j.emc.2017.01.002.
[6] R.B. Schoene, Illnesses at high altitude, Chest 134 (2008) 402–416, https://doi.org/10.1378/chest.07-0561.
[7] S. Paul, A. Gangwar, K. Bhargava, Y. Ahmad, D4f prophylaxis enables redox and energy homeostasis while preventing inflammation during hypoxia exposure, Biomed. Pharmacother. 133 (2021), 111083, https://doi.org/10.1016/j.biopha.2020.111083.
[8] M. Yamamoto, T.W. Kensler, H. Motohashi, The keap1-nrf2 system: a thiol-based sensor-effector apparatus for maintaining redox homeostasis, Physiol. Rev. 98 (2018) 1169–1203, https://doi.org/10.1152/physrev.00023.2017.
[9] C. Lisk, J. McCord, S. Bose, T. Sullivan, Z. Loomis, E. Nozik-Grayck, T. Schroeder, K. Hamilton, D.C. Irwin, Nrf2 activation: a potential strategy for the prevention of acute mountain sickness, Free. Radic. Biol. Med. 63 (2013) 264–273, https://doi.org/10.1016/j.freeradbiomed.2013.05.024.
[10] M. Gao, J. Yi, J. Zhu, A.M. Minikes, P. Monian, C.B. Thompson, X. Jiang, Role of mitochondria in ferroptosis, Mol. Cell 73 (2019) 354–363, https://doi.org/10.1016/j.molcel.2018.10.042.
[11] X. Wang, H. Sun, L. Cui, X. Wang, C. Ren, Z. Tong, X. Ji, Acute high-altitude hypoxia exposure causes neurological deficits via formaldehyde accumulation, CNS Neurosci. Ther. 28 (2022) 1183–1194, https://doi.org/10.1111/cns.13849.
[12] F. Kuang, J. Liu, D. Tang, R. Kang, Oxidative damage and antioxidant defense in ferroptosis, Front. Cell. Dev. Biol. 8 (2020), 586578, https://doi.org/10.3389/fcell.2020.586578.
[13] A. Lewinska, J. Adamczyk-Grochala, D. Bloniarz, B. Horeczy, S. Zurek, A. Kurowicki, B. Woloszczuk-Gebicka, K. Widenka, M. Wnuk, Remifentanil preconditioning protects against hypoxia-induced senescence and necroptosis in human cardiac myocytes in vitro, Aging 12 (2020) 13924–13938, https://doi.org/10.18632/aging.103604.
[14] S. Haga, A. Kanno, T. Ozawa, N. Morita, M. Asano, M. Ozaki, Detection of necroptosis in ligand-mediated and hypoxia-induced injury of hepatocytes using a novel optic probe-detecting receptor-interacting protein (rip)1/rip3 binding, Oncol. Res. 26 (2018) 503–513, https://doi.org/10.3727/096504017×15005102445191.
[15] B. Zhang, H.S. Chang, K.L. Hu, X. Yu, L.N. Li, X.Q. Xu, Combination of geniposide and eleutheroside b exerts antidepressant-like effect on lipopolysaccharide-induced depression mice model, Chin. J. Integr. Med. 27 (2021) 534–541, https://doi.org/10.1007/s11655-019-3051-5.
[16] F. Wang, C. Yuan, B. Liu, Y.F. Yang, H.Z. Wu, Syringin exerts anti-breast cancer effects through pi3k-akt and egfr-ras-raf pathways, J. Transl. Med. 20 (2022) 310, https://doi.org/10.1186/s12967-022-03504-6.
[17] H. Dong, M. Wu, Y. Wang, W. Du, Y. He, Z. Shi, Total syntheses and anti-inflammatory activities of syringin and its natural analogues, J. Nat. Prod. 84 (2021) 2866–2874, https://doi.org/10.1021/acs.jnatprod.1c00585.
[18] Z. Shen, C. Yang, P. Zhu, C. Tian, A. Liang, Protective effects of syringin against oxidative stress and inflammation in diabetic pregnant rats via tlr4/myd88/nf-κb signaling pathway, Biomed. Pharmacother. 131 (2020), 110681, https://doi.org/10.1016/j.biopha.2020.110681.
[19] A. Zhang, Z. Liu, L. Sheng, H. Wu, Protective effects of syringin against lipopolysaccharide-induced acute lung injury in mice, J. Surg. Res. 209 (2017) 252–257, https://doi.org/10.1016/j.jss.2016.10.027.
[20] H. Zang, Q. Yang, J. Li, Eleutheroside b protects against acute kidney injury by activating igf pathway, Molecules 24 (2019), https://doi.org/10.3390/molecules24213876.
[21] J. Xu, Z. Peng, R. Li, T. Dou, W. Xu, G. Gu, Y. Liu, Z. Kang, H. Tao, J.H. Zhang, R. P. Ostrowski, J. Lu, X. Sun, Normoxic induction of cerebral hif-1alpha by acetazolamide in rats: role of acidosis, Neurosci. Lett. 451 (2009) 274–278, https://doi.org/10.1016/j.neulet.2009.01.008.
[22] H. Zhang, H. Gu, Q. Jia, Y. Zhao, H. Li, S. Shen, X. Liu, G. Wang, Q. Shi, Syringin protects against colitis by ameliorating inflammation, Arch. Biochem. Biophys. 680 (2020), 108242, https://doi.org/10.1016/j.abb.2019.108242.
[23] S. Qiu, P. Li, H. Zhao, X. Li, Maresin 1 alleviates dextran sulfate sodium-induced ulcerative colitis by regulating nrf2 and tlr4/nf-kb signaling pathway, Int. Immunopharmacol. 78 (2020), 106018, https://doi.org/10.1016/j.intimp.2019.106018.

[24] J. Ma, C. Wang, Y. Sun, L. Pang, S. Zhu, Y. Liu, L. Zhu, S. Zhang, L. Wang, L. Du, Comparative study of oral and intranasal puerarin for prevention of brain injury induced by acute high-altitude hypoxia, Int. J. Pharm. 591 (2020), 120002, https://doi.org/10.1016/j.ijpharm.2020.120002.
[25] J. Tan, C. Gao, C. Wang, L. Ma, X. Hou, X. Liu, Z. Li, Expression of aquaporin-1 and aquaporin-5 in a rat model of high-altitude pulmonary edema and the effect of hyperbaric oxygen exposure, Dose Response 18 (2020), https://doi.org/10.1177/1559325820970821.
[26] R.M. McGuigan, P. Mullenix, L.L. Norlund, D. Ward, M. Walts, K. Azarow, Acute lung injury using oleic acid in the laboratory rat: establishment of a working model and evidence against free radicals in the acute phase, Curr. Surg. 60 (2003) 412–417, https://doi.org/10.1016/s0149-7944(02)00775-4.
[27] K.S.S. S, H.P. Veeramohan, T. Mathew, C.M. S. S, Nifedipine inhibits hypoxia induced transvascular leakage through down regulation of nfkb, Respir. Physiol. Neurobiol. 183 (2012) 26–34, https://doi.org/10.1016/j.resp.2012.05.016.
[28] J. Shi, Z. Liu, M. Li, J. Guo, L. Chen, L. Ding, X. Ding, T. Zhou, J. Zhang, Polysaccharide from Potentilla anserina l ameliorate pulmonary edema induced by hypobaric hypoxia in rats, Biomed. Pharmacother. 139 (2021), 111669, https://doi.org/10.1016/j.biopha.2021.111669.
[29] S.J. Dixon, K.M. Lemberg, M.R. Lamprecht, R. Skouta, E.M. Zaitsev, C.E. Gleason, D.N. Patel, A.J. Bauer, A.M. Cantley, W.S. Yang, B. Morrison 3rd, B.R. Stockwell, Ferroptosis: an iron-dependent form of nonapoptotic cell death, Cell 149 (2012) 1060–1072, https://doi.org/10.1016/j.cell.2012.03.042.
[30] A.M. Luks, E.R. Swenson, P. Bärtsch, Acute high-altitude sickness, Eur. Respir. Rev. 26 (2017), https://doi.org/10.1183/16000617.0096-2016.
[31] J. Vandewalle, A. Luypaert, K. De Bosscher, C. Libert, Therapeutic mechanisms of glucocorticoids, Trends Endocrinol. Metab. 29 (2018) 42–54, https://doi.org/10.1016/j.tem.2017.10.010.
[32] H. Lu, H. Zhang, Y. Jiang, Methazolamide in high-altitude illnesses, Eur. J. Pharm. Sci. 148 (2020), 105326, https://doi.org/10.1016/j.ejps.2020.105326.
[33] E. Ausó, V. Gómez-Vicente, G. Esquiva, Visual side effects linked to sildenafil consumption: an update, Biomedicines 9 (2021), https://doi.org/10.3390/biomedicines9030291.
[34] D. Shukla, S. Saxena, J. Purushothaman, K. Shrivastava, M. Singh, S. Shukla, V. K. Malhotra, S. Mustoori, A. Bansal, Hypoxic preconditioning with cobalt ameliorates hypobaric hypoxia induced pulmonary edema in rat, Eur. J. Pharmacol. 656 (2011) 101–109, https://doi.org/10.1016/j.ejphar.2011.01.038.
[35] C.K. Lin, Y.H. Lin, T.C. Huang, C.S. Shi, C.T. Yang, Y.L. Yang, Vegf mediates fat embolism-induced acute lung injury via vegf receptor 2 and the mapk cascade, Sci. Rep. 9 (2019) 11713, https://doi.org/10.1038/s41598-019-47276-4.
[36] J. Yu, Z. Ma, S. Shetty, M. Ma, J. Fu, Selective hdac6 inhibition prevents tnf-α-induced lung endothelial cell barrier disruption and endotoxin-induced pulmonary edema, Am. J. Physiol. Am. J. Physiol. Lung. Cell. Mol. Physiol. 311 (2016) L39–L47, https://doi.org/10.1152/ajplung.00051.2016.
[37] D.Y. Zheng, M. Zhou, J. Jin, M. He, Y. Wang, J. Du, X.Y. Xiao, P.Y. Li, A.Z. Ye, J. Liu, T.H. Wang, Inhibition of p38 mapk downregulates the expression of il-1β to protect lung from acute injury in intestinal ischemia reperfusion rats, Mediat. Inflamm. 2016 (2016), 9348037, https://doi.org/10.1155/2016/9348037.
[38] M.P. Grocott, D.S. Martin, D.Z. Levett, R. McMorrow, J. Windsor, H. E. Montgomery, Arterial blood gases and oxygen content in climbers on mount everest, N. Engl. J. Med. 360 (2009) 140–149, https://doi.org/10.1056/NEJMoa0801581.
[39] A. Tripathi, P.P. Hazari, A.K. Mishra, B. Kumar, S.S.K. Sagi, Quercetin: a savior of alveolar barrier integrity under hypoxic microenvironment, Tissue Barriers 9 (2021), 1883963, https://doi.org/10.1080/21688370.2021.1883963.
[40] M.H. Ahmed, M.S. Ghatge, M.K. Safo, Hemoglobin: structure, function and allostery, Subcell. Biochem. 94 (2020) 345–382, https://doi.org/10.1007/978-3-030-41769-7_14.
[41] C.Y. Wang, Q. Zhang, Z. Xun, L. Yuan, R. Li, X. Li, S.Y. Tian, N. Xin, Y. Xu, Increases of iaspp-keap1 interaction mediated by syringin enhance synaptic plasticity and rescue cognitive impairments via stabilizing nrf2 in alzheimer's models, Redox Biol. 36 (2020), 101672, https://doi.org/10.1016/j.redox.2020.101672.
[42] B. Zhang, W. Niu, D. Xu, Y. Li, M. Liu, Y. Wang, Y. Luo, P. Zhao, Y. Liu, M. Dong, R. Sun, H. Dong, Z. Li, Oxymatrine prevents hypoxia- and monocrotaline-induced pulmonary hypertension in rats, Free. Radic. Biol. Med. 69 (2014) 198–207, https://doi.org/10.1016/j.freeradbiomed.2014.01.013.
[43] J. Ren, J. Li, J. Hu, H. Yu, Q. Yang, J. Mu, Overexpression of ckip-1 alleviates hypoxia-induced cardiomyocyte injury by up-regulating nrf2 antioxidant signaling via keap1 inhibition, Biochimie 163 (2019) 163–170, https://doi.org/10.1016/j.biochi.2019.06.008.
[44] J. Patel, B.A. Baptiste, E. Kim, M. Hussain, D.L. Croteau, V.A. Bohr, DNA damage and mitochondria in cancer and aging, Carcinogenesis 41 (2020) 1625–1634, https://doi.org/10.1093/carcin/bgaa114.
[45] S. Li, P. Wu, B. Han, Q. Yang, X. Wang, J. Li, N. Deng, B. Han, Y. Liao, Y. Liu, Z. Zhang, Deltamethrin induces apoptosis in cerebrum neurons of quail via promoting endoplasmic reticulum stress and mitochondrial dysfunction, Environ. Toxicol. 37 (2022) 2033–2043, https://doi.org/10.1002/tox.23548.
[46] Q. Chen, L. Zhu, K.M. Yip, Y. Tang, Y. Liu, T. Jiang, J. Zhang, Z. Zhao, T. Yi, H. Chen, A hybrid platform featuring nanomagnetic ligand fishing for discovering cox-2 selective inhibitors from aerial part of saussurea laniceps hand.-mazz, J. Ethnopharmacol. 271 (2021), 113849, https://doi.org/10.1016/j.jep.2021.113849.
[47] G. Valacchi, A. Pecorelli, C. Cervellati, J. Hayek, 4-hydroxynonenal protein adducts: Key mediator in rett syndrome oxinflammation, Free. Radic. Biol. Med. 111 (2017) 270–280, https://doi.org/10.1016/j.freeradbiomed.2016.12.045.
[48] I. Liguori, G. Russo, F. Curcio, G. Bulli, L. Aran, D. Della-Morte, G. Gargiulo, G. Testa, F. Cacciatore, D. Bonaduce, P. Abete, Oxidative stress, aging, and diseases, Clin. Interv. Aging 13 (2018) 757–772, https://doi.org/10.2147/cia.S158513.
[49] Li, Y. Cao, J. Xiao, J. Shang, Q. Tan, F. Ping, W. Huang, F. Wu, H. Zhang, X. Zhang, Inhibitor of apoptosis-stimulating protein of p53 inhibits ferroptosis and alleviates intestinal ischemia/reperfusion-induced acute lung injury, Cel. Death Differ. 27 (2020) 2635–2650, https://doi.org/10.1038/s41418-020-0528-x.
[50] D. Chen, O. Tavana, B. Chu, L. Erber, Y. Chen, R. Baer, W. Gu, Nrf2 is a major target of arf in p53-independent tumor suppression, Mol. Cell 68 (2017) 224–232, https://doi.org/10.1016/j.molcel.2017.09.009.
[51] Z. Zhang, M. Guo, Y. Li, M. Shen, D. Kong, J. Shao, H. Ding, S. Tan, A. Chen, F. Zhang, S. Zheng, Rna-binding protein zfp36/ttp protects against ferroptosis by regulating autophagy signaling pathway in hepatic stellate cells, Autophagy 16 (2020) 1482–1505, https://doi.org/10.1080/15548627.2019.1687985.
[52] H.S. Kain, E.K.K. Glennon, K. Vijayan, N. Arang, A.N. Douglass, C.L. Fortin, M. Zuck, A.J. Lewis, S.L. Whiteside, D.R. Dudgeon, J.S. Johnson, A. Aderem, K. R. Stevens, A. Kaushansky, Liver stage malaria infection is controlled by host regulators of lipid peroxidation, Cell Death Differ. 27 (2020) 44–54, https://doi.org/10.1038/s41418-019-0338-1.
[53] Y. Wang, S. Yan, X. Liu, F. Deng, P. Wang, L. Yang, L. Hu, K. Huang, J. He, Prmt4 promotes ferroptosis to aggravate doxorubicin-induced cardiomyopathy via inhibition of the nrf2/gpx4 pathway, Cell Death Differ. (2022), https://doi.org/10.1038/s41418-022-00990-5.
[54] H. Dong, Z. Qiang, D. Chai, J. Peng, Y. Xia, R. Hu, H. Jiang, Nrf2 inhibits ferroptosis and protects against acute lung injury due to intestinal ischemia reperfusion via regulating slc7a11 and ho-1, Aging 12 (2020) 12943–12959, https://doi.org/10.18632/aging.103378.
[55] G. Wang, S. Qin, Y. Zheng, C. Xia, P. Zhang, L. Zhang, J. Yao, Y. Yi, L. Deng, T-2 toxin induces ferroptosis by increasing lipid reactive oxygen species (ros) and downregulating solute carrier family 7 member 11 (slc7a11), J. Agric. Food Chem. 69 (2021) 15716–15727, https://doi.org/10.1021/acs.jafc.1c05393.
[56] N.K. Campbell, H.K. Fitzgerald, A. Dunne, Regulation of inflammation by the antioxidant haem oxygenase 1, Nat. Rev. Immunol. 21 (2021) 411–425, https://doi.org/10.1038/s41577-020-00491-x.
[57] X. Cai, S. Hua, J. Deng, Z. Du, D. Zhang, Z. Liu, N.U. Khan, M. Zhou, Z. Chen, Astaxanthin activated the nrf2/ho-1 pathway to enhance autophagy and inhibit ferroptosis, ameliorating acetaminophen-induced liver injury, ACS Appl. Mater. Interfaces 14 (2022) 42887–42903, https://doi.org/10.1021/acsami.2c10506.
[58] B. Han, S. Li, Y. Lv, D. Yang, J. Li, Q. Yang, P. Wu, Z. Lv, Z. Zhang, Dietary melatonin attenuates chromium-induced lung injury via activating the sirt1/pgc-1α/nrf2 pathway, Food Funct. 10 (2019) 5555–5565, https://doi.org/10.1039/c9fo01152h.
[59] Y. Wu, H. Jiao, Y. Yue, K. He, Y. Jin, J. Zhang, J. Zhang, Y. Wei, H. Luo, Z. Hao, X. Zhao, Q. Xia, Q. Zhong, J. Zhang, Ubiquitin ligase e3 huwe1/mule targets transferrin receptor for degradation and suppresses ferroptosis in acute liver injury, Cell Death Differ. (2022), https://doi.org/10.1038/s41418-022-00957-6.
[60] M. Pasparakis, P. Vandenabeele, Necroptosis and its role in inflammation, Nature 517 (2015) 311–320, https://doi.org/10.1038/nature14191.
[61] Y. Zhou, H. Jin, Y. Wu, L. Chen, X. Bao, C. Lu, Gallic acid protects against ethanol-induced hepatocyte necroptosis via an nrf2-dependent mechanism, Toxicol. In Vitro 57 (2019) 226–232, https://doi.org/10.1016/j.tiv.2019.03.008.
[62] Z. Yang, Y. Wang, Y. Zhang, X. He, C.Q. Zhong, H. Ni, X. Chen, Y. Liang, J. Wu, S. Zhao, D. Zhou, J. Han, Rip3 targets pyruvate dehydrogenase complex to increase aerobic respiration in tnf-induced necroptosis, Nat. Cell. Biol. 20 (2018) 186–197, https://doi.org/10.1038/s41556-017-0022-y.
[63] B.R. Stockwell, J.P. Friedmann Angeli, H. Bayir, A.I. Bush, M. Conrad, S.J. Dixon, S. Fulda, S. Gascón, S.K. Hatzios, V.E. Kagan, K. Noel, X. Jiang, A. Linkermann, M. E. Murphy, M. Overholtzer, A. Oyagi, G.C. Pagnussat, J. Park, Q. Ran, C. S. Rosenfeld, K. Salnikow, D. Tang, F.M. Torti, S.V. Torti, S. Toyokuni, K. A. Woerpel, D.D. Zhang, Ferroptosis: a regulated cell death nexus linking metabolism, redox biology, and disease, Cell 171 (2017) 273–285, https://doi.org/10.1016/j.cell.2017.09.021.
[64] J. Cui, M. Yan, X. Liu, S. Yin, S. Lu, L. Fan, H. Hu, Inorganic selenium induces nonapoptotic programmed cell death in pc-3 prostate cancer cells associated with inhibition of glycolysis, J. Agric. Food Chem. 67 (2019) 10637–10645, https://doi.org/10.1021/acs.jafc.9b03875.
[65] Y. Zhang, S.S. Su, S. Zhao, Z. Yang, C.Q. Zhong, X. Chen, Q. Cai, Z.H. Yang, D. Huang, R. Wu, J. Han, Rip1 autophosphorylation is promoted by mitochondrial ros and is essential for rip3 recruitment into necrosome, Nat. Commun. 8 (2017), 14329, https://doi.org/10.1038/ncomms14329.
[66] A.B. Nair, S. Jacob, A simple practice guide for dose conversion between animals and human, J. Basic. Clin. Pharm. 7 (2016) 27–31, https://doi.org/10.4103/0976-0105.177703.